HHS Public Access

Author manuscript

J Am Chem Soc. Author manuscript; available in PMC 2020 October 30.

Published in final edited form as:

J Am Chem Soc. 2019 October 30; 141(43): 17025–17041. doi:10.1021/jacs.9b09149.

Molecular MR Imaging with Gd(III)-based Agents: Challenges and Key Advances

Hao Li[1], **Thomas J. Meade**[1]

[1]Departments of Chemistry; Molecular Biosciences; Neurobiology; and Radiology Northwestern University, Evanston, IL 60208

Abstract

In an era of personalized medicine, the clinical community has become increasingly focused on understanding diseases at the cellular and molecular level. Magnetic resonance imaging (MRI) is a powerful imaging modality for acquiring anatomical and functional information. However, it has limited applications in field of molecular imaging due to low sensitivity. To expand the capability of MRI to encompass molecular imaging applications, we introduced bioresponsive Gd(III)-based magnetic resonance contrast agents (GBCAs) in 1997. Since that time, many research groups across the globe have developed new examples of biopresponsive GBCAs. These contrast agents have shown great promise for visualizing several biochemical processes such as gene expression, neuronal signaling and hormone secretion. They are designed to be conditionally retained, or activated, *in vivo* in response to specific biochemical events of interest. As a result, an observed MR signal change can serve as a read-out for molecular events. A significant challenge for these probes is how to utilize them for noninvasive diagnostic and theranostic applications. This Perspective focuses on the design strategies that underlie bioresponsive probes, and describes the key advances made in recent years that are facilitating their application *in vivo* and ultimately in clinical translation. While the field of bioresponsive agents is embryonic, it is clear that many solutions to the experimental and clinical radiologic problems of today will be overcome by the probes of tomorrow.

Graphical Abstract

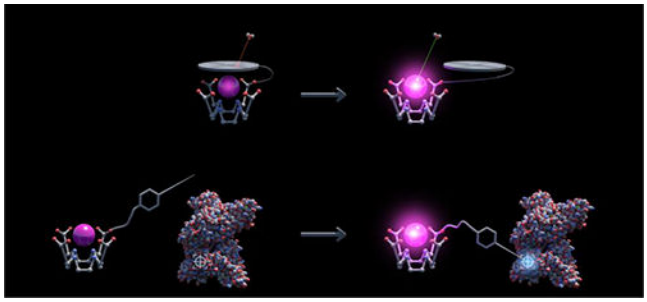

Corresponding Author tmeade@northwestern.edu.

The authors declare no competing financial interest.

INTRODUCTION

Magnetic resonance imaging (MRI) is the modality of choice for evaluating many diseases. It is a staple of clinical diagnostic radiology due to its tunable soft-tissue contrast, high spatial and temporal resolution and lack of ionizing radiation. The use of paramagnetic Gd(III) based MR contrast agents (GBCAs) further enhances anatomical features and improves diagnostic accuracy.[1] Currently, clinically-approved GBCAs are limited to providing anatomical or functional information, and are not capable of affording molecular data.

In order to expand the capability of MRI into the molecular imaging regime,[2] our lab and others have developed a specialized class of contrast agents known as bioresponsive GBCAs.[3] These contrast agents conditionally respond to a biochemical event of interest by altering the MR signal through either selective binding (targeted GBCAs), or biorthogonal chemical transformations (activatable GBCAs). Traditionally, the term “bioresponsive GBCAs” only refers to activatable GBCA but not targeted contrast agents. However, bioresponsive agents are defined as “materials that are sensitive to biological signals or to pathological abnormalities, and interact with, or are actuated by them”,[4] and targeted MR contrast agents interact with molecular biomarkers via selective binding. Thus, we will use the term “bioresponsive GBCAs” to designate both targeted and activatable GBCAs.

Different classes of contrast agents are available for each individual MRI technique. For example, Gd(III) and other paramagnetic metal ions chelates are used for ^{1}H T_1-weighted MRI. Superparamagnetic iron-oxide nanoparticles (SPIONs) are utilized for T_2 and T_2*weighted MRI. Chemical exchange saturation transfer (CEST) contrast agents are used for CEST MRI, and ^{19}F-containing materials are developed for ^{19}F MRI. For a more comprehensive analysis on the above topics, readers are directed to a recent review by Caravan et al..[3e] For the purpose of this Perspective, we will primarily focus on small molecule bioresponsive Gd(III)-based CAs for T_1-weighted ^{1}H MRI because these imaging agents are derived from clinically-approved GBCAs. A few examples of non-Gd(III) CAs will also be discussed as they complement their Gd(III) counterparts.

Gd(III) accelerates the T_1 relaxation of water protons resulting in brighter MR signals in T_1-weighted MRI, which is among the most commonly used MR techniques in medical exams. However, Gd(III) ions are toxic to biological systems and a suitable ligand or chelate must bind the lanthanide to form a bio-unavailable and nontoxic complex. Several factors influence the stability of the GBCA including enthalpy and entropy effects (denticity, charge and basicity of coordinating groups, ligand field, and conformational effects). While there have been notable concerns (Nephrogenic Systemic Fibrosis), clinically used GBCAs have an excellent safety profile with severe adverse events in only 1 in 40,000 injections.[5] As a result, approximately 40% of clinical MR scans employ Gd(III) chelates for contrast-enhanced MRI (> 20 million/year).

The majority of bioresponsive GBCAs are based on chelate scaffolds diethylenetriaminepentaacetic acid (DTPA), 1,4,7,10-tetraazacyclododecane-1,4,7,10-tetraacetic acid (DOTA) and 1,4,7,10-tetraazacyclododecane-1,4,7-triacetic acid (DO3A),

where the R group can be modified to equip the GBCA with molecular imaging capability (Figure 1). The use of cyclen-based macrocyclic ligands, such as DOTA and DO3A, gained popularity over linear ligands such as DTPA due to superior stability as well as ease of functionalization.

Since the development of the first bioresponsive GBCAs two decades ago, numerous examples and design strategies have been reported.[3] However, as noted in a recent review by Angelovski, only a small fraction of these agents have been successfully employed *in vivo*, and none as yet have translated into clinical trials.[6] One goal of this perspective is to understand why this is the case and offer an assessment of how this may change in the future. We begin with a discussion of the essentials of the relaxation theory of GBCAs and introduce key parameters dictating GBCA-enhanced MR signals. We illustrate how these parameters can be manipulated by different activation/targeting strategies, supported by reports from the literature. Finally, we discuss the current limitations of bioresponsive GBCAs and the recent efforts that will circumvent these key issues.

1. RELAXATION THEORY FOR GBCAs

The radiocontrast agents used in CT and radiotracers used in PET/SPECT generate the observed signal directly. However, GBCAs provide contrast indirectly by reducing the longitudinal relaxation time (T_1) and the transverse relaxation time (T_2) of water protons, which translates to brighter (T_1-weighted) or darker (T_2-weighted) MR images. Water protons have intrinsic T_1 and T_2 values that are often referred to as the *diamagnetic* components of signal, $T_{1,d}$ and $T_{2,d}$. Therefore, varying soft tissues with distinct $T_{1,d}$ and $T_{2,d}$ values can be resolved via MRI without the use of contrast agents.[7]

In contrast to the diamagnetic water protons, GBCAs are *paramagnetic*, and their Brownian motion in aqueous environment generates fluctuating magnetic fields that accelerate the T_1 and T_2 relaxations of nearby water protons. This phenomenon is known as paramagnetic relaxation enhancement (PRE). From a chemical perspective, we can manipulate the PRE effect of GBCAs to alter the observed MR signals. For this perspective, we will focus on T_1 PRE because GBCAs are rarely used as T_2 agents.

Longitudinal Relaxivity (r_1)—The overall T_1-weighted MR signal intensity is correlated to the observed T_1 relaxation rate of water protons ($1/T_{1,obs}$, eq 1), which equals to the sum of diamagnetic contribution of water protons and the paramagnetic component from GBCAs. The paramagnetic contribution of GBCAs is further broken down to the product of longitudinal relaxivity (r_1) and the concentration of Gd(III). r_1 (in $mM^{-1}s^{-1}$) is the degree to which GBCAs decrease the T_1 of water protons as a function of Gd(III) concentration. It describes the efficiency of the GBCA at relaxing water protons. On the other hand, the concentration of the GBCA is positively correlated to the overall PRE effect, and this concentration-dependence of PRE effect is a key factor to designing targeted GBCAs (Section 2). To put eq 1 into perspective, at clinical field strength (1.5 T) without any GBCAs, $1/T_{1,obs} = 1/T_{1,d}$ which for freely diffusing water is about 0.3 s^{-1}; however, in the presence of 1 mM of FDA-approved GBCA Dotarem with $r_1 = 2.9\ mM^{-1}\ s^{-1}$, $1/T_{1,obs} = 0.3 + 2.9 \times 1 = 3.2\ s^{-1}$, which corresponds to a 10-fold signal enhancement.

Inner-sphere Relaxivity (r_1^{IS}).—The relaxivity (r_1) can be factored into outer-sphere relaxivity r_1^{OS} and inner-sphere relaxivity r_1^{IS} (eq 2). r_1^{OS} comes from PRE on water molecules that are hydrogen bonded to the GBCA as well as those that are further away. r_1^{IS} comes from PRE on water molecules *directly bound* to the metal center and the water molecules that are rapidly exchanging with the metal-bound water molecule. The outer-sphere effect is still not well understood despite accounting for about 40% of the overall relaxivity in small molecule GBCAs.[8] This presents a huge challenge for activatable GBCAs as it leads to persistent off-state background signals. For the purpose of this review, we will primarily focus on inner-sphere parameters because they are more readily manipulated by changing the chemical structure of the ligand. As shown in eq 3, the inner-sphere relaxivity (r_1^{IS}) is related to three key terms: q, τ_m, and T_{1m} which is dominated by τ_R (Figure 2)

Hydration Number (q).: q is the number of water molecules directly bound to the Gd(III) center (the hydration number) and is directly proportional to r_1^{IS} (eq 3). Most GBCAs have up to 2 coordination sites open for direct water coordination. Further increasing the hydration number is often associated with decreased stability.[3e, 9] Note that measured q value is often a non-integer as it is the average of a bulk property. Modulating q was used in designing the first activatable GBCA and remains a popular choice for designing activatable GBCAs (Section 3).[3a]

Water Residency Time (τ_m).: To transfer the strong PRE of Gd(III) to nearby water, the metal-bound water molecule rapidly exchanges with the bulk water molecules. The water residency time (τ_m) is typically on the order of 100 ns for a typical cyclen-based Gd(III) complex.[10] In other words, one molecule of GBCA relaxes roughly ten million water molecules per second. For most small molecules GBCAs, $\tau_m \ll T_{1m}$, and eq 3 can be simplified to eq 4.

***T_1* of the Metal-bound Water (T_{1m}).:** T_{1m} is the T_1 of the Gd(III)-bound water molecule and is described by the Solomon-Bloembergen-Morgan paramagnetic relaxation theory.[11] At a field strength above 0.1 T, T_{1m} is described by eq 5 where C is a constant, $r_{Gd(III)H}$ is the Gd(III)-water proton distance, τ_c is the correlation time for magnetic fluctuation induced by Gd(III), and ω_H is the Lamor frequency of proton. Two important conclusions can be drawn from eq 5: (1) T_{1m} is very sensitive to $r_{Gd(III)H}$, and shorter $r_{Gd(III)H}$ leads to higher $1/T_{1m}$; (2) $1/T_{1m}$ is maximized when τ_c^{-1} approaches $2\pi\omega_H$ (eq 6). The latter is because the dipolar interaction between the water protons and the electron spins of the Gd(III) is responsible for the T_1 PRE. This electron spin-nuclear interaction is at the strongest when both the magnetic moment of water proton (described by Larmor frequency) and the magnetic field induced by Gd(III) electron spins (described by τ_c^{-1}) fluctuate at similar frequencies, as shown in eq 6.

τ_c^{-1} is the sum of three terms: i) T_{1e}^{-1}, where T_{1e} is the electronic relaxation time intrinsic to the metal and estimated to be ~10 ns at 0.5 T for Gd(III), while being much longer at higher field;[10] ii) τ_m^{-1}, where τ_m is the water residency time and is about 100 ns for Gd(III)-DOTA and Gd(III)-DO3A; III) τ_R^{-1} where τ_R is the rotational correlation time on the order of 0.1 ns for small molecule GBCAs (eq 7).[10] The key conclusion here is that τ_R dominates τ_c^{-1} and therefore is the major parameter determining T_{1m} as well as r_1^{IS}.[12] We will

consider two field strengths, 0.5 T (low field) and 9.4 T (high field), to see why this is the case.

$$\frac{1}{T_{1,\mathrm{obs}}} = \frac{1}{T_{1,\mathrm{d}}} + r_1[\mathrm{Gd(III)}] \tag{1}$$

$$r_1 = r_1^{\mathrm{OS}} + r_1^{\mathrm{IS}} \tag{2}$$

$$r_1^{\mathrm{IS}} = \frac{q/[\mathrm{H_2O}]}{T_{1m} + \tau_m} \tag{3}$$

$$r_1^{\mathrm{IS}} \cong \frac{q/[\mathrm{H_2O}]}{T_{1m}} \text{ if } T_{1m} \gg \tau_m \tag{4}$$

$$\frac{1}{T_{1m}} = \frac{\mathrm{C}}{r_{Gdh}^6} \times \frac{\frac{6\pi}{\tau_c}}{\frac{1}{\tau_c^2} + 4\pi^2\omega_H^2} \tag{5}$$

$$\frac{1}{T_{1m}} \text{ is at maximum when } \frac{1}{\tau_c} = 2\pi\omega_H \tag{6}$$

$$\frac{1}{\tau_c} = \frac{1}{\tau_R} + \frac{1}{\tau_m} + \frac{1}{T_{1e}} \tag{7}$$

Low Field 0.5–1.5 T.: At 0.5 T (21 MHz for ^{1}H) the optimal τ_c to maximize relaxivity is 7.6 ns according to eq 6. As a mathematical consequence of eq 7, the *smallest* of the three terms (T_{1e}, τ_m, τ_R) dictates the value of τ_c. For a small molecule GBCA, because τ_R (0.1 ns) ≪ T_{1e} (10 ns) < τ_m (100 ns), τ_R dictates τ_c ($\tau_c = \tau_R$ = 0.1 ns) and it is much smaller than the optimal 7.6 ns. This is the main reason why small molecule GBCA with q =1 have r_1 in the range of 3–5 $mM^{-1}s^{-1}$, which is far less than the theoretical maximum (~100 $mM^{-1}s^{-1}$) at low field. Conversely, increasing τ_R by either tethering the GBCA to a biomacromolecules (Section 2) or triggering the self-assembly of a specially designed GBCA (Section 3.2) are two very effective methods for developing bioresponsive GBCAs. As τ_R increases by 1–2 orders of magnitude from 0.1 ns to 1–10 ns, the τ_c will correspondingly approach 1–10 ns and get much closer to the optimal 7.6 ns. This allows for more efficient Gd(III)-induced relaxation of water protons, and therefore higher r_1.

High Field 7–9.4 T.: At high field 9.4 T (400 MHz for ^{1}H), the optimal τ_c is 0.4 ns according to eq 6. At this field strength, T_{1e} of Gd(III) is longer than 10 ns and has no

significant influence on τ_c or r_1. Within a broad range of values (10–1000 ns) τ_m does not significantly affect r_1 either.[13] Therefore, it is τ_R that again dictates the value of τ_c.

In contrast to low field, at high field the optimal τ_R to achieve high relaxivity is in the range of 0.1–1 ns. This corresponds to a τ_c of roughly 0.1–1 ns, close to the optimal 0.4 ns. Further increasing τ_R to 10 ns, for example, pushes the τ_c to 5–10 ns, which is no longer close to the optimal 0.4 ns. The effect of τ_R on T_1 relaxivity at different field strengths is shown in figure 3.[13] Due to the relatively small range of τ_R that can effectively change r_1 at high field, it is *rare* to use τ_R change for developing bioresponsive GBCAs at high field. Instead, manipulating q or the concentration of GBCAs are much more common strategies for designing bioresponsive or targeted GBCAs since both terms affect r_1 in a field-independent manner.

From the above discussion, we can extrapolate the terms that can be used to manipulate the r_1 of GBCAs. Specifically, both q and [Gd(III)] are linearly correlated with $1/T_{1obs}$ and independent of the field strength. Increasing τ_R can significantly impact the r_1 at low field, and is also a viable option at high field, though rarely used. In some cases, one bioresponsive GBCA may utilize several bioresponsive strategies working synergistically to increase the observed MR signal. In the following sections we will describe the chemical strategies used to impact changes in r_1.

2. TARGETED GBCAs

Targeted GBCAs involve conjugating a targeting ligand to a Gd(III) chelate (Figure 4). This allows the GBCA to bind selectively to the target biomarker, usually a protein that is more abundant in the disease state than in the healthy state. The targeting strategy increases the MR signal via the differential accumulation of the GBCAs. As the biomacromolecule-bound GBCAs are retained, the unbound ones are quickly cleared out. Additionally, the receptor-bound GBCA usually has increased r_1 compared to the unbound GBCA as a result of increased τ_R, further enhancing the MR signal. This binding-induced MR signal enhancement is referred to as the receptor-induced magnetization enhancement (RIME) effect.[14]

Several key factors need to be considered when designing an effective targeted GBCA: (1) the location and abundance of the target biomarker; (2) whether a multimeric approach is required to achieve the necessary sensitivity for detection; (3) the optimal distance between the ligand and GBCA to achieve both strong binding and high r_1 in the biomacromolecule-bound form.

2.1 Imaging target selection for targeted GBCAs—

The relatively low sensitivity of ^{1}H MRI is the major obstacle for targeted MRI. Because most targeted GBCAs rely on stoichiometric binding with the biomarker, the concentration of the biomarker determines the amount of GBCAs present at the target site. Since the sensitivity of ^{1}H MRI is in the range of μM, biomarkers that are in the pM-nM range may not be imaged with targeted GBCAs.[15] These ranges are far better suited for PET/SPECT imaging that has the necessary probe sensitivity. In the following sections we categorize biomarkers of interest via their locations, namely: extracellular targets, cell surface receptors, and intracellular targets.

Extracellular Biomarkers.: Imaging extracellular targets does not require efficient cellular uptake of targeted GBCAs. As such, highly abundant extracellular biomarkers such as protons (pH),[16] serum albumin,[14c, 17] and burst release of metal ions[18] (section 3.1) are preferred molecular MRI targets. For other targets of unknown concentrations, it is recommended to estimate their abundance and determine if targeted MRI is applicable. For example, Caravan et al. reported an oxyamine-based GBCA targeting the allysines formed in lung fibrogenesis (Figure 5A).[19] They quantified the amount of allysine to be approximately 80 μM in normal mice, and 150 μM in diseased mice. Such high μM concentrations permitted MR detection via small molecule GBCAs, and their lead probe GdOA was successfully applied *in vivo* to image lung fibrosis in mice (Figure 5B).

Cell surface receptors.: Targeting receptors overexpressed on the cell surface to identify a specific cell population (such as malignant cells) is another powerful application for targeted GBCAs. As with imaging extracellular targets, it is crucial to estimate the concentration of the receptors on the cell surface. As opposed to extracellular targets that bind targeted GBCAs stoichiometrically, these receptor proteins on the cell surface can internalize into cells, carrying the receptor-bound GBCAs with them via receptor-mediated endocytosis. Subsequently, these receptors can recycle back to the cell surface to shuffle more targeted GBCAs into the cells, further increasing the intracellular concentration of the targeted GBCAs.

Internalization of GBCAs through receptor-mediated endocytosis can play a vital role in targeted MRI. Pomper et al. developed a series of GBCAs that target the prostate-specific membrane antigen (PSMA) overexpressed in primary and metastatic prostate cancer.[20] Three targeted GBCAs were studied, namely Gd1, Gd2 and Gd3, with 1, 2 or 3 Gd(III) chelates conjugated to the urea PSMA-targeting ligand (Figure 6A). The multimeric approach was effective at increasing intracellular Gd(III) concentration. When incubated with PC3 PIP (PSMA+) cells, Gd1, Gd2 and Gd3 had an estimated intracellular Gd(III) concentration of 7.2 μM, 12.5 μM and 22.8 μM, respectively. Non-specific uptake in PC3 flu (PSMA-) cells was low. Subsequently, Gd3 was used for MRI of PIP and flu tumor xenografts in mice (Figure 6B). T_1-contrast enhancement remained constant for about 3 h within the PC3 PIP (PSMA+) tumor while decreasing rapidly within the PC3 flu (PSMA-) tumor (Figure 6C).

Targeted GBCAs have been shown to enter cells through receptor-mediated endocytosis.[21] A caveat of this approach is that the GBCA taken up in this manner can be trapped inside the endosomes. This can severely attenuate the MR signal or even lead to the degradation of GBCAs.[22] An alternative approach is to target other protein-mediated internalization processes that do not involve endosomes, such as organic anion transporting peptides (OATPs).[23]

Non-internalizing surface receptors and intracellular proteins.: The same principle applies to imaging cellular proteins: it is essential to estimate their concentrations. For example, we attempted to image HaloTags expressed on the surface of HT+ cells (engineered to express HaloTag).[24] We estimated that the HT+ cells have a concentration of 1.6–0.4 μM HaloTag on the cell surface. Although this concentration of HaloTag is at the

high end of mammalian proteome, a one-Gd(III)-one-ligand construct is insufficient to achieve significant MR signal enhancement. As a result, a small molecule multimeric approach where serval Gd(III) chelates are conjugated to one targeting ligand, or a nanoparticle approach where hundreds of Gd(III) chelates are conjugated to the particle surface needs to be employed. In this case, the latter approach was used.[24]

The above study raises an important question: what cellular proteins are in the concentrations detectable via one-Gd(III)-one-ligand GBCAs? Assuming the MRI detection limit is 10 μM, this translates to a minimum of 1.1×10^7 target proteins per cell. According to an important study published by Selbach et al. that quantifies mammalian cells' protein expression, cellular proteins with such high concentrations are typically nuclear proteins (such as histones), ribosomal proteins, structural proteins (actin, tubulin), and heat shock proteins.[25]

In other words, these are mostly house-keeping proteins and are not attractive imaging targets. Imaging intracellular targets with MRI is further beset by the difficulty of having GBCAs effectively penetrate the cellular membrane, a key issue discussed later. To our knowledge, successfully using MRI to detect an intracellular target with small molecule targeted GBCAs has yet to be reported. As a result, the importance of a multimeric/ nanoparticle approach becomes increasingly clear.

2.2 Selecting the appropriate linker.—For targeted GBCAs, the linker length needs to be optimized to achieve both tight binding as well as a high r_1 in the bound form. If the Gd(III) chelate too close it might interfere with the ligand-receptor interaction; if too far apart, the *internal motion* of the Gd(III) chelate becomes significant, compromising the RIME effect.[15] If the two components are infinitely far away from each other, they become two separate entities and the slow rotation of the ligandreceptor complex is completely decoupled from the fast internal motion of the Gd(III) chelate.

To balance between binding affinity and internal motion, an intermediate distance between the Gd(III) chelate and the ligand is optimal. For example, we reported a series of GBCAs that target HaloTag, a gene reporter protein develop by Promega (Figure 7).[26] HaloTag is a hydrolase engineered to covalently bind to a chloroalkane substrate. This chloroalkane targeting group was conjugated to Gd(III)-DO3A with 1–4 methylene groups in between (n = 1 to 4), corresponding to 1CHTGd, 2CHTGd, 3CHTGd, and 4CHTGd. It was discovered that 2CHTGd possess both optimal binding and maximal relaxivity increase upon binding to HaloTag (from 7.6 to 22.0 $mM^{-1}s^{-1}$). This exemplifies the necessity of optimizing the distance between the Gd(III) chelate and the targeting group when designing a targeted MR probe.

It is important to note that the RIME effect is weak at high field strengths (>3 T), which are routinely used for preclinical MRI. Upon binding to a biomacromolecule such as a protein, the τ_R of the probe-protein complex would increase to >10 ns, outside the range of optimal τ_R (0.1–1 ns) needed to achieve maximum r_1 at high field. If high field MRI is required, the linker should be tuned to primarily optimize binding rather than relaxivity change.

3. ACTIVATABLE GBCAs

In contrast to targeted GBCAs that selectively bind to a biomarker of interest, activatable GBCAs rely on the relaxivity change upon a chemical reaction elicited by enzyme activities, pH change, metal ion binding, or different redox potentials. These reactions change the MR parameters (q and τ_R are most common) of the GBCA, thereby switching the activatable GBCA from "off-state" to "on-state". In this section, we will discuss the design strategy for activatable GBCAs, as well as several non-Gd(III)-based magnetic resonance contrast agents (MRCAs), and how they can be employed to image a variety of biological and pathological processes.

3.1. *q*-modulated activatable GBCAs—

Because of the linear relationship between q and r_1, an increase in q after bioactivation of a GBCA corresponds to an increased r_1. In the off-state, water molecules have restricted access to the Gd(III) metal center due to a capping ligand blocking coordination, leading to a q of 0 or 1. In the on-state, the capping ligand is lifted through binding of a biological metal ion, or is cleaved off by a biological enzyme (Figure 8). As a result, q increases as does the MR signal.

Imaging enzymatic activity.: In contrast to receptor proteins that can only bind to a set number of ligands, enzymes can turn over hundreds to millions copies of substrate rapidly, thereby improving the detection limit by several orders of magnitude. A classic example for q-modulated enzyme-responsive GBCA is the β-galactosidase (β-Gal) imaging agent developed by our lab and referred to as the Egad series.[3a, 27] These Gd(III) complexes are based on the DO3A ligand of which the N-10 position is modified with a two-carbon linker to galactopyranose (Figure 9A, top). Egad has two methylene carbons as the linker and is designed to detect β-galactosidase (β-gal), an enzyme that is commonly used in molecular biology as a reporter for target gene expression.[28] Prior to activation, the galactopyranose "capped" the Gd(III) metal center restricting water access. Post-activation, the sugar is cleaved by β-gal and water molecules can directly bind to the Gd(III) ion.

The first of the series was Egad (Figure 9A, top). The measured q of Egad vs. the activated agent was 0.7 and 1.2, respectively, translating to a 20% decrease in T_1 when Egad was incubated with β-Gal. The flexible linker was thought to be responsible for the relatively small change in T_1 upon activation.

To rigidify the linker, a methyl group was introduced at the α and β positions in two Egad derivatives, α-EgadMe and β-EgadMe (Figure 9A, middle and bottom).[27] Interestingly, these two probes had distinct activation mechanisms. While α-EgadMe was activated through the same capping-uncapping mechanism as Egad, β-EgadMe had a carbonate anion bound to the Gd(III), creating a low q complex prior to activation. Upon cleavage of the sugar, the remaining hydroxyl group chelated with Gd(III) to replace the carbonate, creating a coordination site for water. Upon activation, the r_1 of β-EGadMe increased from 0.9 to 2.72 $mM^{-1}s^{-1}$ providing observable contrast *in vivo*.

As expected, β-EGadMe was successfully applied *in vivo* for MRI detection of β-gal mRNA expression in living X.laevis embryos (Figure 9B).[27a] Both embryos were injected with β-EGadMe. The embryo on the right was also given β-gal mRNA and showed a 45–60%

higher MR signal than the other embryo without β-gal mRNA. This was the first *in vivo* demonstration of an activatable GBCA, signifying the potential of using activatable GBCA to monitor a specific biological process *in vivo*.

As demonstrated by β-EGadMe, anions present in the biological media such as carbonate, bicarbonate and phosphate can act as bidentate ligand and bind to the stable q of 2 Gd(III)-DO3A complex, attenuating the MR signal enhancement.[14b, 29] To avoid this issue it is possible to use specialized ligands designed to minimize anion coordination to the lanthanide.[30] In other cases, the anion coordination can be utilized to quench the "off-state" signal. For example an esterase-sensitive GBCA was developed with this strategy (Figure 10).[31] Prior to activation, carbonate binds to the DO3A-based Gd(III) chelate forming the "off-state." Upon esterase activation, three negatively charged carboxylates are exposed, displacing the carbonate via charge-charge repulsion. With the carbonate absent, water molecules have access to the Gd(III) center to form a q of 2 complex (Figure 10).

This capping-uncapping activation mechanism has been used to develop many other activatable GBCAs that report on enzyme activity and other biological targets. Readers are referred to more comprehensive reviews of these agents.[3c, 3e]

Metal ion sensing.: Another class of q-modulated GBCAs employ known ligands that bind to biologically active metal to affect changes in the hydration state of Gd(III) (Figure 11). As such, these agents are usually designed to sense biological metal ions.

The first example reported by our group was a q-modulated Ca(II)-sensitive probe, DOPTA-Gd (Figure 12).[32] It had a bismacrocylic structure with two Gd(III)-DO3A chelates on each side and a Ca(II)-binding ligand (BAPTA) at the center. In the absence of Ca(II), the carboxylates of the BAPTA ligand coordinated to the two Gd(III) ions leading to a low q of 0.6. In the presence of Ca(II), the BAPTA preferentially bound to Ca(II) over Gd(III), increasing q to 2.1. As a result, DOPTA-Gd showed a 75% increase in relaxivity in the presence of Ca(II) at physiologically relevant concentrations (0.1–10 μM).

Metal sensing GBCAs show a reversible interaction with the metal ions, and the MR signal can be correlated with the ion concentration. The dynamic range of the agent is related to the dissociation constant (K_d) of the metal-binding ligand. For example, DOPTA-Gd is responsive to Ca(II) concentration from 0.1–10 μM with a K_d of 0.96 μM, mimicking the K_d of BAPTA (0.2 μM). This makes BATPA suitable for monitoring the intracellular Ca(II) level (low μM). The same principles apply when designing bioresponsive MR probes for other biological metals such as Zn[18] and Cu,[33] as well as pH[16] and even neurotransmitters.[34]

3.2. τ_R-modulated GBCAs—

For most small molecule GBCAs, a short rotational correlation time τ_R is the limiting factor to achieve high relaxivity (especially at a low field strength). If the activatable GBCA forms larger complexes that tumble slower in solution, the resulting τ_R will be increased. This allows for more efficient Gd(III)-induced relaxation of water protons, hence selectively enhancing r_1. Additionally, because larger complexes often have slower clearance *in vivo* compared to low molecular weight small molecules, τ_R-modulated GBCAs often have concomitant enhanced accumulation/retention that further

boost the observed MR signal. In the following section we will discuss two main τ_R-based activation strategies and their applications *in vivo*.

Activation-binding: Activation-binding strategy, also known as activation-targeting or activation-retention, is a one-two punch process. In the first step, the agent undergoes a chemical change in response to the biological target. It then acquires the ability to bind to a protein, such as human serum albumin (HSA), thereby increasing the τ_R, r_1, as well as retention (Figure 13).

For example, the Sherry group has reported a series of Zn(II)-sensitive GBCAs that, upon binding with Zn(II), acquires the ability to interact with HSA.[18c, 18d, 18f] These probes are comprised of a Gd(III)-DO3A conjugated to a Zn(II)-binding ligand that can be modulated to fine-tune the Zn(II) binding affinity. Because Zn(II) also bind strongly to HSA, it connects Zn(II)-sensitive GBCAs and HSA together to form a ternary complex (Figure 14B). Two most recently reported agents, GdL1 and GdL2 had K_d = 118 nM and 2350 nM for Zn(II) (Figure 14A).[18f] In the presence of Zn(II) and mouse serum albumin at 9.4 T, the r_1 of GdL1 increased from 4.1 to 6.1 $mM^{-1}s^{-1}$, while the r_1 of GdL2 increased from 4.0 to 5.6 $mM^{-1}s^{-1}$. Both agents were used *in vivo* to monitor the transient Zn(II) release from pancreatic β-cells upon glucose stimulation (Figure 14C). Because GdL2 had a lower K_d, it binds only weakly to endogenous free Zn(II), leading to a lower MR signal background and an overall larger MR signal change upon activation compared to GdL1 (Figure 14D).

Self-assembly/aggregation.: A bioresponsive self-assembly or aggregation of the GBCA can also lead to increased τ_R and r_1. These MR probes usually contain reactive groups that react inter- or intra-molecularly upon activation to form higher-order assemblies, thereby increasing the τ_R (Figure 15).

An early example is MPO-Gd reported by Weissleder et al. for tracking myeloperoxidase (MPO) activities, a key inflammatory enzyme secreted by activated immune cells such as neutrophils and macrophages.[35] A typical MPO- is comprised of two 5hydroxytryptamide (5-HT) groups conjugated to Gd(III)-DTPA. In the presence of MPO, 5-HT groups are oxidized, radicalized and then react intermolecularly to form oligomers up to 5 subunits (Figure 16A).[35a] The radicals formed can also react with proteins nearby, causing prolonged retention of the agent as well as r_1 increase. MPO-Gd was shown to enhance the MR signal in a mouse myocardial infarction model. Strong and persistent MR signal enhancement was observed in the infarct zone in mice injected with MPO-Gd, but not with Gd(III)-DTPA (Figure 16B&C), indicating that MPO-Gd was activated *in vivo* through elevated MPO activity at the infarct zone.[35a]

In addition to from radical polymerization, controlled self-assembly of conditionally activated small molecules is another promising approach for designing τ_R-modulated MR probes. The Rao group developed a caspase-sensitive nano-aggregation MRI probe (C-SNAM) for monitoring caspase-3/7-mediated apoptosis.[36] Both caspases are activated during apoptosis to carry out mass proteolysis. As a result, elevated caspase-3/7 activities serve as unique biomarkers for apoptosis. Monitoring their activities provides invaluable information for tumor therapy as well as preclinical anticancer drug selection. However,

because caspase-3/7 are located intracellularly, the designed imaging probe must enter cells efficiently to access the enzymes, an issue that will be discussed later (Section 4.1).

C-SNAM consists of a 2-cyano-6-hydroxyquinoline (CHQ) and a D-cysteine residue for efficient biocompatible cyclization, a DEVD peptide recognized by active caspase-3/7, a disulfide bond to be reduced by intracellular glutathione (GSH), and a Gd(III)-DOTA monoamide chelate as the GBCA (Figure 17). In the presence of caspase-3/7 and intracellular GSH, C-SNAM undergoes intramolecular cyclization to form a macrocycle. Because the macrocycle is rigid and hydrophobic, in aqueous solution it can further assemble into Gd(III) nanoparticles that have increased τ_R and r_1. In the presence of caspase-3 and GSH, C-SNAM showed an increase in r_1 from 10.2 to 19.0 $mM^{-1}s^{-1}$. As such, C-SNAM was used to detect apoptosis of matrix-associated stem cell implanted in rat knee joints.[36b]

4. MAJOR CONSIDERATIONS FOR ACTIVATABLE GBCAs

Since a variety of activation strategies are available when designing bioresponsive GBCAs, observing a turn-on response of GBCA *in vitro* is no longer a challenging task. However, effectively observing the signal change *in vivo* and correlating it with the biochemical process in question is far more challenging mainly due to the low sensitivity of MRI probes. In this section, we will discuss major considerations regarding imaging target selection and methods to quantify the “turn-on” response *in vivo*. We believe this section will serve as a guideline for designing new biorepsonsive agents and inspire innovative strategies that will enhance the sensitive of these *in vivo* imaging probes.

4.1 Target selection for activatable GBCAs—

As with targeted GBCAs, selecting the appropriate biomarker is the crucial factor for determining whether the molecular MRI can be successfully applied *in vivo*. It is also important to note that different activation strategies are suited for different imaging targets. Herein, we will discuss three key factors concerning imaging target selection: location of the imaging target, resolution and timescale required for the selected biochemical process, and the cellular uptake of the GBCAs.

Extracellular and cell surface biomarkers.: The accessibility of the imaging target depends on its location. In general, the ease of access to a contrast agent is as follows: extracellular targets > cell surface proteins > intracellular targets. As a result, extracellular pH, metabolites as well as enzymes and metal ions that are secreted from the cells are preferable targets for activatable GBCAs. Additionally, some cell surface receptors have enzymatic activities that makes them ideal targets for activatable GBCAs.

For example, γ-glutamyltranspeptidase (GGT) is a cell-surface associated enzyme that catalyzes the cleavage of a γ-glutamyl bond of glutathione, and it was found to be overexpressed in several cancers. Liang et al. reported a GGT-responsive T_2-based activatable MR probe **1** (Figure 18A).[37] Upon activation by GGT and intracellular GSH, **1** forms dimers that are hydrophobic and further assemble into nanoparticles, with r_2 increased from 5.79 to 25.1 $mM^{-1}s^{-1}$ (Figure 18A). As such, **1** was used for T_2-weighteded MRI of HeLa tumor-bearing mice. The T_2-weighted MR contrast of tumors in **1**-injected mice peaked at 2.5 h post-injection, whereas only a minor signal decrease was observed with mice

pretreated with GGT inhibitor 6-diazo-5-oxo-L-norleucine (DON) and then with **1**, or mice injected with Gd(III)-DTPA (Figure 18 B & C).

Intracellular biomarkers.: Because most enzymes are intracellular, efficient cellular delivery of the bioresponsive GBCAs is the first step to successfully monitoring enzyme activity. A large body of literature focuses on cellular delivery of GBCAs with a variety of strategies, including cell penetrating peptides,[38] nanomaterials,[39] and many other delivery platforms.[40] However, effective cellular delivery of small molecule bioresponsive GBCAs remains challenging. Because most GBCAs are hydrophilic/negatively charged, they are unlikely to penetrate the cellular membrane via passive diffusion. If incubated at high concentrations, GBCAs can be taken up via pinocytosis, a process in which the cell engulfs the extracellular fluid along with the small particles/molecules in it.[41] However, pinocytosis is a non-specific mechanism when compared to ligand-specific receptor-mediated endocytosis. As a result, relying on pinocytosis for cellular uptake leads to poor selectivity and also requires a large amount of agent around the target cell population for an extended period. This is difficult to achieve *in vivo* as small molecules usually have a short *in vivo* half-life.

The low membrane permeability of GBCAs have prompted the development of alternative CAs that are more likely to penetrate cells. Specifically, several membrane-permeable Mn-based magnetic resonances contrast agents (MRCAs) have been developed.[42] For example, the Lippard and Jasanoff groups reported a Mn-based bioresponsive MRCA for intracellular Ca(II) sensing.[43] The manganese-based intracellular Ca(II) sensor (ManICS1-AM) structure was based on a previously reported Mn(II) scaffold attached to an acetoxymethyl ester (AM ester) derivatized BAPTA (Figure 19A). Once inside the cells, intracellular esterases would hydrolyze the AM esters, unmasking the BAPTA ligand to liberate the sensor in its “off” state. In this state, the carboxylate on the BAPTA is expected to bind with the Mn(II), leading to low MR signal. However, once the BAPTA binds to intracellular Ca(II), the q of the sensor would increase leading to MR signal enhancement (Figure 19A). They demonstrated that cells labeled with ManICS1-AM showed MR signal enhancement when treated with chemical agents known to change intracellular Ca(II) level. Furthermore, ManICS1-AM was used to detect Ca(II) level fluctuation *in vivo*. ManICS1-AM was injected intracranially and produced persisting contrast enhancement for over 90 mins, suggesting intracellular trapping of the probe. Subsequently, a high concentration of KCl was infused to the brain to depolarize neurons and increase intracellular calcium concentrations. This elicited a 5.8% MR signal change proximal to the infusion site in ManICS1-AM-infused brain areas (Figure 19B&C). Although the change is small, it is substantially higher than that of a Ca(II)-insensitive control probe (MnL1F) or when NaCl instead of KCl was used (Figure 19B&C). Because Mn-based MRCAs possess superior cell permeability and similar relaxivity compared to those of GBCAs, we expect more Mn-based activatable MR probes to be developed in the future for imaging intracellular processes.

4.2 Spatial resolution and temporal resolution—A typical MRI scanner has spatial resolution in the hundreds of micrometers with 1mm slice thickness, while ultra-high-field MRI can reach resolutions in the tens of micrometers (approximately the diameter of a

mammalian cell).[44] As a result, MRI can be used to detect at nearly single cell resolution, albeit requiring extremely "bright" MRCAs.[45] For small molecule GBCAs with r_1 = 4 mM $^{-1}s^{-1}$ at high field, it is nearly impossible to achieve single-cell resolution. It is important to keep this in mind when choosing the imaging target.

Additionally, the time scale of biological process is a key factor to consider for molecular MRI. A standard spin-echo sequence for constructing a T_1 map takes minutes to complete; while a rapid series of T_1-weighted fast low angle shot magnetic resonance imaging (FLASH MRI) scans take a few seconds to tens of seconds. Thus, very transient biological processes might need specialized pulse sequences. This is especially important when imaging metal ion fluxes which may have a "spike" of high metal concentration with a duration less than 1s.[46]

4.3 MR signal quantification—For targeted MRI using a concentration-dependent approach, a strong MR signal can be reliably correlated with the high concentration of biomarkers. However, this is not the case for activatable GBCAs that rely on change in r_1 to evaluate the target biomarker. Because the "off-state" of the probe also has MR signal, MR signal enhancement cannot always be assigned solely to activated probes versus the pooling of the inactive agents. This is the so-called MR signal quantification problem, which entails quantifying the concentrations of probes that are in the "on" and "off" states.

The most common method to validate the MR "turn-on" response *in vivo* is to use a control probe that is a non-responsive analogue of the activatable agent.[19, 36a] The control probe is assumed to have the same biodistribution profile as a responsive one, and therefore can be used to estimate the concentration of the responsive probe under similar *in vivo* conditions. However, a minor structural change can still have a significant impact on an agent's pharmacokinetic profile. In this section we will focus on the innovative methods developed to quantify the MR signal enhancement without using a control probe.

Increasing the dynamic range.: Since a false positive arises from the background MR signal of the parent probe, making the "off state" agent truly "dark" is the obvious solution. However, it is challenging to minimize the r_1 of a Gd(III) chelate. As a proof-of-concept, our group has demonstrated using magnetic coupling interaction between Co(II) and Gd(III) to lower the r_1 of GBCA.[47] When the paramagnetic Co(II) shares an oxo ligand with Gd(III), it can shorten the T_{1e} of Gd(III) through intramolecular magnetic exchange coupling and reduce the r_1 at low field (1.5 T). However, this method is unlikely to be effective at high field and is yet to be applied in *in vivo*.

Quenching the "off-state" of the MRCA has been demonstrated with other paramagnetic metal ions complexes. For Mn, Fe and Eu, switching between oxidation states is feasible and can have a huge effect on r_1 of the resulting MRCAs.[48] Recently, the Caravan group reported a striking example of a redox active iron complex, Fe-PyC3A (Figure 20A).[48e]

It had an impressive ten-fold increase in r_1 as Fe oxidation state was switched from (II) to (III), at all three field strengths measured (1.4, 4.7, 11.7 T). The "off state" is Fe(II)-PyC3A had a r_1 of merely 0.15 $mM^{-1}s^{-1}$ at 11.7 T. This is because low spin Fe(II) is diamagnetic,

and therefore incapable of producing paramagnetic enhancement. However, once oxidized to the paramagnetic Fe(III), the r_1 of the complex increased to 2.2 $mM^{-1}s^{-1}$, comparable to that of Gd(III)-based contrast agents. As such, the redox active Fe-PyC3A was successfully applied *in vivo* to image the oxidative stress during acute inflammation (Figure 20B). Nonetheless, a major constraint of this strategy is that it is limited to imaging redox potentials.

Multimodal imaging.: Another method is to use a bimodal agent where another imaging modality of higher sensitivity is used to quantify the concentration of the MR agents. PET has excellent sensitivity and PET-MRI bimodal scanners are available for simultaneous measurement of both MR and PET signals. This has been demonstrated *in vitro* for pH sensing.[49] A similar approach has been applied using SPECT signal to quantify the MR probe concentration.[50]

Fluorescence imaging can be used to quantify MRI experiments.[51] In contrast to PET/SPECT probes, fluorescent probes can be readily designed to be bioresponsive. One can design a fluorescence-magnetic resonance (FL-MR) bioresponsive probe that exhibits simultaneous FL-MR signal enhancement after activation. Because fluorogenic probes have excellent sensitivity and large dynamic range, the FL signal change can be used to substantiate the MR signal enhancement in response to the biological stimulus. We have recently reported a bimodal fluorescence-magnetic resonance (FL-MR) probe CP1 (caspase probe-1) that exhibits simultaneous FL-MR turn-on response to caspase-3/7, and showed that the FL signal of CP1 can be used to quantify the concentrations of the active and inactive probes *in vitro*.[52] However, for *in vivo* applications of FL-MR probes, the limited depth penetration of FL imaging as well as the different sensitivities of two imaging modalities need to be considered. Since PET-MRI scanners have been commercialized and are gaining popularity in the clinic we expect new PET-MRI bioresponsive MRCAs to be developed in the future.

Improved Pulse Sequence Technology.: The development of new MRI pulse sequences can facilitate MR signal quantification.[53] When a bioresponsive GBCAs is “activated” both the r_1 and r_2 are impacted. As a result, if both the r_1 and r_2 of the MR probe before and after activation are known, it is possible quantify the concentration of the agent before and after activation. One powerful technology that can rapidly measure both T_1 and T_2 in the same field of view is magnetic resonance fingerprinting (MRF).[54] This technique introduced by Griswold et al. permits the simultaneous quantification of multiple MR properties of a material or tissue. Instead of using a repeated, serial acquisition of data for T_1 and T_2 mapping, MRF uses a pseudorandomized acquisition that causes the signals from different materials or tissues to have a unique MR signal “fingerprint.” This unique signature is simultaneously a function of the multiple material properties (T_1 and T_2) under investigation. Through data processing, these properties can be quantified by matching the MR fingerprint of the material/tissue to a predefined dictionary of predicted MR parameters. The best-matched MR parameters would be used to quantify the MR properties of the material/tissue of interest.

Because MRF can be used to quantify T_1 and T_2 in the field of view simultaneously and with high temporal resolution, if the r_1 and r_2 of the on- and off-probes are known, MRF can be used to quantify the concentration of both agents. Flask et al. confirmed this possibility as they were able to use MRF to simultaneously quantify the concentration of two distinct MRI contrast agents during one acquisition.[55] Currently, this approach is being applied to bioresponsive agents and utilize MRF to quantify the concentrations of activatable GBCAs in both “off” and “on” states.

CONCLUSIONS AND OUTLOOK

Bioresponsive GBCAs have the potential to noninvasively probe and investigate essential physiological and pathological processes at the molecular level by MRI. To realize this potential, it is imperative that researchers from chemistry, biology, biomedical engineering and clinicians collaborate to overcome the obstacles described here. The roadmap for a successful *in vivo* application of bioresponsive GBCAs must begin with selecting the appropriate target biomarkers, which requires a strong biological and clinical background. Subsequently, the design, synthesis and *in vitro* evaluation of the bioresponsive GBCAs will require chemists with organic, inorganic and MR physics expertise. Finally, researchers with a biomedical imaging background are required to carry out the *in vivo* imaging experiments, so that the appropriate MRI hardware as well as pulse sequences can be used to maximize the chance for successful *in vivo* applications. To further advance bioresponsive GBCAs towards clinical translation requires scientists with medical and medicinal chemistry backgrounds. It is important to ensure that these GBCAs not only have good efficacy but also has little to no longterm side effects, especially for GBCAs that are retained in the body for prolonged period. Like many scientific endeavors, the field of bioresponsive GBCAs is highly interdisciplinary, and only with close collaboration will new breakthroughs be possible.

Here, we have described the relaxation theory of bioresponsive GBCAs and how various parameters can be manipulated to design this class of agents. For both targeted and activatable GBCAs, choosing the appropriate biomarker is of utmost importance. In general, biomarkers that are extracellular and abundant (high μM range) are preferred targets. Imaging intracellular targets can be accomplished with activatable GBCAs due to the signal amplification. However, when probing intracellular phenomena, activatable GBCAs need to be made more cell-permeable and this remains an ever-present obstacle.

A unique challenge for developing new activatable MR probes is to unambiguously correlate MR signal enhancement with a biological event under investigation. It is encouraging to see the numerous recent advances in GBCA design, new MR pulse sequences, and hybrid imaging modalities that are providing promising solutions for this exciting field.

ACKNOWLEDGMENTS

H.L. and T.J.M. acknowledge support by NIH Grant P30CA060553.

REFERENCES

1. (a)Carr DH; Brown J; Bydder GM; Weinmann HJ; Speck U; Thomas DJ; Young IR Intravenous Chelated Gadolinium as a Contrast Agent in NMR Imaging of Cerebral-Tumors. Lancet 1984, 1, 484–486; [PubMed: 6142210] (b)Helm L; Merbach AE; Tóth E. v.; ProQuest (Firm), The Chemistry of Contrast Agents in Medical Magnetic Resonance Imaging. 2nd ed.; John Wiley & Sons Inc.: Hoboken, N.J., 2013 http://ebookcentral.proquest.com/lib/northeastern-ebooks/detail.action?docID=1132797.
2. Weissleder R; ProQuest (Firm), Molecular Imaging Principles and Practice. People's Medical Pub. House: Shelton, Conn., 2009 http://ebookcentral.proquest.com/lib/northeasternebooks/detail.action?docID=3386912.
3. (a)Moats RA; Fraser SE; Meade TJA "Smart" Magnetic Resonance Imaging Agent That Reports on Specific Enzymatic Activity. Angew Chem Int Edit 1997, 36, 726–728;(b)Heffern MC; Matosziuk LM; Meade TJ Lanthanide Probes for Bioresponsive Imaging. Chem. Rev 2014, 114, 4496–539; [PubMed: 24328202] (c)Hingorani DV; Bernstein AS; Pagel MD A Review of Responsive MRI Contrast Agents: 2005–2014. Contrast Media Mol. Imaging 2015, 10, 245–265; [PubMed: 25355685] (d)Lux J; Sherry AD Advances in Gadolinium-Based MRI Contrast Agent Designs for Monitoring Biological Processes in Vivo. Curr. Opin. Chem. Biol 2018, 45, 121–130; [PubMed: 29751253] (e)Wahsner J; Gale EM; Rodriguez-Rodriguez A; Caravan P Chemistry of MRI Contrast Agents: Current Challenges and New Frontiers. Chem. Rev 2019, 119, 957–1057; [PubMed: 30350585] (f)Que EL; Chang CJ Responsive Magnetic Resonance Imaging Contrast Agents as Chemical Sensors for Metals in Biology and Medicine. Chem. Soc. Rev 2010, 39, 51–60. [PubMed: 20023836]
4. Lu Y; Aimetti AA; Langer R; Gu Z Bioresponsive Materials. Nat Rev Mater 2017, 2.
5. Prince MR; Zhang HL; Zou ZT; Staron RB; Brill PW Incidence of Immediate Gadolinium Contrast Media Reactions. Am. J. Roentgenol 2011, 196, W138–W143. [PubMed: 21257854]
6. Angelovski G What We Can Really Do with Bioresponsive MRI Contrast Agents. Angew Chem Int Edit 2016, 55, 7038–7046.
7. Bojorquez JZ; Bricq S; Acquitter C; Brunotte F; Walker PM; Lalande A What Are Normal Relaxation Times of Tissues at 3 T? Magn. Reson. Imaging 2017, 35, 69–80. [PubMed: 27594531]
8. (a)Hwang LP; Freed JH Dynamic Effects of Pair Correlation-Functions on Spin Relaxation by Translational Diffusion in Liquids. J. Chem. Phys 1975, 63, 4017–4025;(b)Borel A; Helm L; Merbach AE Molecular Dynamics Simulations of MRI-Relevant Gd-III Chelates: Direct Access to Outer-Sphere Relaxivity. Chem. Eur. J 2001, 7, 600–610; [PubMed: 11261657] (c)De Leon-Rodriguez LM; Martins AF; Pinho MC; Rofsky NM; Sherry AD Basic MR Relaxation Mechanisms and Contrast Agent Design. J. Magn. Reson. Imaging 2015, 42, 545–565. [PubMed: 25975847]
9. Port M; Idee JM; Medina C; Robic C; Sabatou M; Corot C Efficiency, Thermodynamic and Kinetic Stability of Marketed Gadolinium Chelates and Their Possible Clinical Consequences: A Critical Review. Biometals 2008, 21, 469–490. [PubMed: 18344005]
10. Caravan P; Ellison JJ; McMurry TJ; Lauffer RB Gadolinium(III) Chelates as MRI Contrast Agents: Structure, Dynamics, and Applications. Chem. Rev 1999, 99, 2293–2352. [PubMed: 11749483]
11. (a)Solomon I; Bloembergen N Nuclear Magnetic Interactions in the Hf Molecule. J. Chem. Phys 1956, 25, 261–266;(b)Bloembergen N Proton Relaxation Times in Paramagnetic Solutions. J. Chem. Phys 1957, 27, 572–573;(c)Bloembergen N; Morgan LO Proton Relaxation Times in Paramagnetic Solutions Effects of Electron Spin Relaxation. J. Chem. Phys 1961, 34, 842–850.
12. Laurent S; Elst LV; Muller RN Comparative Study of the Physicochemical Properties of Six Clinical Low Molecular Weight Gadolinium Contrast Agents. Contrast Media Mol. Imaging 2006, 1, 128–137. [PubMed: 17193689]
13. Caravan P; Farrar CT; Frullano L; Uppal R Influence of Molecular Parameters and Increasing Magnetic Field Strength on Relaxivity of Gadolinium- and Manganese-Based T(1) Contrast Agents. Contrast Media Mol. Imaging 2009, 4, 89–100. [PubMed: 19177472]
14. (a)Aime S; Botta M; Crich SG; Giovenzana GB; Pagliarin R; Piccinini M; Sisti M; Terreno E Towards MRI Contrast Agents of Improved Efficacy. NMR Relaxometric Investigations of the Binding Interaction to Hsa of a Novel Heptadentate Macrocyclic Triphosphonate Gd(III)-

Complex. J. Biol. Inorg. Chem 1997, 2, 470–479;(b)Aime S; Gianolio E; Terreno E; Giovenzana GB; Pagliarin R; Sisti M; Palmisano G; Botta M; Lowe MP; Parker D Ternary Gd(III) L-Hsa Adducts: Evidence for the Replacement of Inner-Sphere Water Molecules by Coordinating Groups of the Protein. Implications for the Design of Contrast Agents for MRI. J. Biol. Inorg. Chem 2000, 5, 488–497; [PubMed: 10968620] (c)Caravan P; Cloutier NJ; Greenfield MT; McDermid SA; Dunham SU; Bulte JWM; Amedio JC; Looby RJ; Supkowski RM; Horrocks WD; McMurry TJ; Lauffer RB The Interaction of Ms-325 with Human Serum Albumin and Its Effect on Proton Relaxation Rates. J. Am. Chem. Soc 2002, 124, 3152–3162. [PubMed: 11902904]

15. Caravan P Strategies for Increasing the Sensitivity of Gadolinium Based MRI Contrast Agents. Chem. Soc. Rev 2006, 35, 512–523. [PubMed: 16729145]
16. (a)Zhang SR; Wu KC; Sherry AD A Novel pH-Sensitive MRI Contrast Agent. Angew Chem Int Edit 1999, 38, 3192–3194;(b)Woods M; Kiefer GE; Bott S; Castillo-Muzquiz A; Eshelbrenner C; Michaudet L; McMillan K; Mudigunda SDK; Grin D; Tircso G; Zhang SR; Zhao P; Sherry AD Synthesis, Relaxometric and Photophysical Properties of a New pH-Responsive MRI Contrast Agent: The Effect of Other Ligating Groups on Dissociation of a P-Nitrophenolic Pendant Arm. J. Am. Chem. Soc 2004, 126, 9248–9256; [PubMed: 15281814] (c)Kalman FK; Woods M; Caravan P; Jurek P; Spiller M; Tircso G; Kiraly R; Brucher E; Sherry AD Potentiometric and Relaxometric Properties of a Gadolinium-Based MRI Contrast Agent for Sensing Tissue pH. Inorg. Chem 2007, 46, 5260–5270; [PubMed: 17539632] (d)Ali MM; Woods M; Caravan P; Opina ACL; Spiller M; Fettinger JC; Sherry AD Synthesis and Relaxometric Studies of a Dendrimer-Based pH-Responsive MRI Contrast Agent. Chem. Eur. J 2008, 14, 7250–7258; [PubMed: 18601236] (e)Giovenzana GB; Negri R; Rolla GA; Tei L Gd-Aminoethyl-Do3a Complexes: A Novel Class of pH-Sensitive MRI Contrast Agents. Eur. J. Inorg. Chem 2012, 2035–2039.
17. (a)Lauffer RB; Parmelee DJ; Dunham SU; Ouellet HS; Dolan RP; Witte S; McMurry TJ; Walovitch RC Ms-325: Albumin-Targeted Contrast Agent for Mr Angiography. Radiology 1998, 207, 529–538; [PubMed: 9577506] (b)Cavagna FM; Lorusso V; Anelli PL; Maggioni F; de Haen C Preclinical Profile and Clinical Potential of Gadocoletic Acid Trisodium Salt (B22956/1), a New Intravascular Contrast Medium for MRI. Acad. Radiol 2002, 9, S491–S494; [PubMed: 12188318] (c)La Noce A; Stoelben S; Scheffler K; Hennig J; Lenz HM; La Ferla R; Lorusso V; Maggioni F; Cavagna F B22956/1, a New Intravascular Contrast Agent for MRI: First Administration to Humans - Preliminary Results. Acad. Radiol 2002, 9, S404–S406; [PubMed: 12188290] (d)Paetsch I; Huber ME; Bornstedt A; Schnackenburg B; Boesiger P; Stuber M; Fleck E; Cavagna F; Nagel E Improved Three-Dimensional Free-Breathing Coronary Magnetic Resonance Angiography Using Gadocoletic Acid (B-22956) for Intravascular Contrast Enhancement. J. Magn. Reson. Imaging 2004, 20, 288–293; [PubMed: 15269955] (e)Eldredge HB; Spiller M; Chasse JM; Greenwood MT; Caravan P Species Dependence on Plasma Protein Binding and Relaxivity of the Gadolinium-Based MRI Contrast Agent Ms-325. Invest. Radiol 2006, 41, 229–243. [PubMed: 16481905]
18. (a)Hanaoka K; Kikuchi K; Urano Y; Nagano T Selective Sensing of Zinc Ions with a Novel Magnetic Resonance Imaging Contrast Agent. J Chem Soc Perk T 2 2001, 1840–1843;(b)Major JL; Parigi G; Luchinat C; Meade TJ The Synthesis and in Vitro Testing of a Zinc-Activated MRI Contrast Agent. Proc. Natl. Acad. Sci. U. S. A 2007, 104, 13881–13886; [PubMed: 17724345] (c)Esqueda AC; Lopez JA; Andreu-De-Riquer G; Alvarado-Monzon JC; Ratnakar J; Lubag AJM; Sherry AD; De Leon-Rodriguez LM A New Gadolinium-Based MRI Zinc Sensor. J. Am. Chem. Soc 2009, 131, 11387–11391; [PubMed: 19630391] (d)Lubag AJM; De Leon-Rodriguez LM; Burgess SC; Sherry AD Noninvasive MRI of Beta-Cell Function Using a Zn2+-Responsive Contrast Agent. Proc. Natl. Acad. Sci. U. S. A 2011, 108, 18400–18405; [PubMed: 22025712] (e)Jordan MVC; Lo ST; Chen SW; Preihs C; Chirayil S; Zhang SR; Kapur P; Li WH; De Leon-Rodriguez LM; Lubag AJM; Rofsky NM; Sherry AD Zinc-Sensitive MRI Contrast Agent Detects Differential Release of Zn(Ii) Ions from the Healthy Vs. Malignant Mouse Prostate. Proc. Natl. Acad. Sci. U. S. A 2016, 113, E5464–E5471; [PubMed: 27562169] (f)Martins AF; Jordan VC; Bochner F; Chirayil S; Paranawithana N; Zhang SR; Lo ST; Wen XD; Zhao PY; Neeman M; Sherry AD Imaging Insulin Secretion from Mouse Pancreas by MRI Is Improved by Use of a Zinc-Responsive MRI Sensor with Lower Affinity for Zn2+ Ions. J. Am. Chem. Soc 2018, 140, 17456–17464. [PubMed: 30484648]

19. Waghorn PA; Jones CM; Rotile NJ; Koerner SK; Ferreira DS; Chen HH; Probst CK; Tager AM; Caravan P Molecular Magnetic Resonance Imaging of Lung Fibrogenesis with an Oxyamine-Based Probe. Angew Chem Int Edit 2017, 56, 9825–9828.

20. Banerjee SR; Ngen EJ; Rotz MW; Kakkad S; Lisok A; Pracitto R; Pullambhatla M; Chen ZP; Shah T; Artemov D; Meade TJ; Bhujwalla ZM; Pomper MG Synthesis and Evaluation of Gd-III-Based Magnetic Resonance Contrast Agents for Molecular Imaging of Prostate-Specific Membrane Antigen. Angew Chem Int Edit 2015, 54, 10778–10782.

21. Yuan Z; Li WT; Ye XD; Liu SY; Xiao XS Folate Receptor-Mediated Targeted Polymeric Gadolinium Complexes for Magnetic Resonance Imaging in Pulmonary Tumor Xenografts. Exp. Ther. Med 2012, 3, 903–907. [PubMed: 22969991]

22. Di Gregorio E; Gianolio E; Stefania R; Barutello G; Digilio G; Aime S On the Fate of MRI Gd-Based Contrast Agents in Cells. Evidence for Extensive Degradation of Linear Complexes Upon Endosomal Internalization. Anal. Chem 2013, 85, 5627–5631. [PubMed: 23738707]

23. (a)de Haen C; La Ferla R; Maggioni F Gadobenate Dimeglumine 0.5 M Solution for Injection (Multihance (R)) as Contrast Agent for Magnetic Resonance Imaging of the Liver: Mechanistic Studies in Animals. J. Comput. Assist. Tomogr 1999, 23, S169–S179; [PubMed: 10608413] (b)Van Montfoort JE; Stieger B; Meijer DKF; Weinmann HJ; Meier PJ; Fattinger KE Hepatic Uptake of the Magnetic Resonance Imaging Contrast Agent Gadoxetate by the Organic Anion Transporting Polypeptide Oatp1. J. Pharmacol. Exp. Ther 1999, 290, 153–157; [PubMed: 10381771] (c)Leonhardt M; Oswald S; Adam U; Siegmund W; Weitschies W In Vitro Uptake of the Magnetic Resonance Imaging Contrast Agent Gadoxetate Is Mediated by the Human Hepatic Uptake Carrier Organic Anion-Transporting Polypeptide 1b3. Drug Metab. Rev 2009, 41, 24–24.

24. Vistain LF; Rotz MW; Rathore R; Preslar AT; Meade TJ Targeted Delivery of Gold Nanoparticle Contrast Agents for Reporting Gene Detection by Magnetic Resonance Imaging. Chem. Commun 2016, 52, 160–163.

25. (a)Schwanhausser B; Busse D; Li N; Dittmar G; Schuchhardt J; Wolf J; Chen W; Selbach M Global Quantification of Mammalian Gene Expression Control. Nature 2011, 473, 337–342; [PubMed: 21593866] (b)Schwanhausser B; Busse D; Li N; Dittmar G; Schuchhardt J; Wolf J; Chen W; Selbach M Global Quantification of Mammalian Gene Expression Control (Vol 473, Pg 337, 2011). Nature 2013, 495, 126–127. [PubMed: 23407496]

26. (a)Los GV; Encell LP; McDougall MG; Hartzell DD; Karassina N; Zimprich C; Wood MG; Learish R; Ohane RF; Urh M; Simpson D; Mendez J; Zimmerman K; Otto P; Vidugiris G; Zhu J; Darzins A; Klaubert DH; Bulleit RF; Wood KV Hatotag: A Novel Protein Labeling Technology for Cell Imaging and Protein Analysis. ACS Chem. Biol 2008, 3, 373–382; [PubMed: 18533659] (b)Strauch RC; Mastarone DJ; Sukerkar PA; Song Y; Ipsaro JJ; Meade TJ Reporter Protein-Targeted Probes for Magnetic Resonance Imaging. J. Am. Chem. Soc 2011, 133, 16346–16349. [PubMed: 21942425]

27. (a)Louie AY; Huber MM; Ahrens ET; Rothbacher U; Moats R; Jacobs RE; Fraser SE; Meade TJ In Vivo Visualization of Gene Expression Using Magnetic Resonance Imaging. Nat. Biotechnol 2000, 18, 321–325; [PubMed: 10700150] (b)Urbanczyk-Pearson LM; Femia FJ; Smith J; Parigi G; Duimstra JA; Eckermann AL; Luchinat C; Meade TJ Mechanistic Investigation of Beta-Galactosidase-Activated MR Contrast Agents. Inorg. Chem 2008, 47, 56–68. [PubMed: 18072754]

28. (a)DiMRI GP; Lee X; Basile G; Acosta M; Scott G; Roskelley C; Medrano EE; Linskens M; Rubelj I; Pereira-Smith O; et al. A Biomarker That Identifies Senescent Human Cells in Culture and in Aging Skin in Vivo. Proc. Natl. Acad. Sci. U. S. A 1995, 92, 9363–7; [PubMed: 7568133] (b)Gary RK; Kindell SM Quantitative Assay of Senescence-Associated Beta-Galactosidase Activity in Mammalian Cell Extracts. Anal. Biochem 2005, 343, 329–334; [PubMed: 16004951] (c)Juers DH; Matthews BW; Huber RE Lacz Beta-Galactosidase: Structure and Function of an Enzyme of Historical and Molecular Biological Importance. Protein Sci. 2012, 21, 1792–1807. [PubMed: 23011886]

29. (a)Supkowski RM; Horrocks WD Displacement of Inner-Sphere Water Molecules from Eu3+ Analogues of Gd3+ MRI Contrast Agents by Carbonate and Phosphate Anions: Dissociation Constants from Luminescence Data in the Rapid-Exchange Limit. Inorg. Chem 1999, 38, 5616–5619; [PubMed: 11671291] (b)Bruce JI; Dickins RS; Govenlock LJ; Gunnlaugsson T; Lopinski S; Lowe MP; Parker D; Peacock RD; Perry JJB; Aime S; Botta M The Selectivity of Reversible Oxy-Anion Binding in Aqueous Solution at a Chiral Europium and Terbium Center: Signaling of

Carbonate Chelation by Changes in the Form and Circular Polarization of Luminescence Emission. J. Am. Chem. Soc 2000, 122, 9674–9684;(c)Lowe MP; Parker D; Reany O; Aime S; Botta M; Castellano G; Gianolio E; Pagliarin R pH-Dependent Modulation of Relaxivity and Luminescence in Macrocyclic Gadolinium and Europium Complexes Based on Reversible Intramolecular Sulfonamide Ligation. J. Am. Chem. Soc 2001, 123, 7601–7609. [PubMed: 11480981]

30. (a)Messeri D; Lowe MP; Parker D; Botta M A Stable, High Relaxivity, Diaqua Gadolinium Complex That Suppresses Anion and Protein Binding. Chem. Commun 2001, 2742–2743;(b)Datta A; Raymond KN Gd-Hydroxypyridinone (Hopo)-Based High-Relaxivity Magnetic Resonance Imaging (MRI) Contrast Agents. Acc. Chem. Res 2009, 42, 938–947; [PubMed: 19505089] (c)Gale EM; Kenton N; Caravan P [Gd(Cypic3a)(H2o)(2)](−): A Stable, Bis(Aquated) and High-Relaxivity Gd(III) Complex. Chem. Commun 2013, 49, 8060–8062.
31. Giardiello M; Lowe MP; Botta M An Esterase-Activated Magnetic Resonance Contrast Agent. Chem. Commun 2007, 4044–4046.
32. (a)Li WH; Fraser SE; Meade TJ A Calcium-Sensitive Magnetic Resonance Imaging Contrast Agent. J. Am. Chem. Soc 1999, 121, 1413–1414;(b)Li WH; Parigi G; Fragai M; Luchinat C; Meade TJ Mechanistic Studies of a Calcium-Dependent MRI Contrast Agent. Inorg. Chem 2002, 41, 4018–4024. [PubMed: 12132928]
33. (a)Que EL; Chang CJ A Smart Magnetic Resonance Contrast Agent for Selective Copper Sensing. J. Am. Chem. Soc 2006, 128, 15942–15943; [PubMed: 17165700] (b)Que EL; Gianolio E; Baker SL; Wong AP; Aime S; Chang CJ Copper-Responsive Magnetic Resonance Imaging Contrast Agents. J. Am. Chem. Soc 2009, 131, 8527–8536; [PubMed: 19489557] (c)Que EL; Gianolio E; Baker SL; Aime S; Chang CJ A Copper-Activated Magnetic Resonance Imaging Contrast Agent with Improved Turn-on Relaxivity Response and Anion Compatibility. Dalton T 2010, 39, 469–476;(d)Que EL; New EJ; Chang CJ A Cell-Permeable Gadolinium Contrast Agent for Magnetic Resonance Imaging of Copper in a Menkes Disease Model. Chem. Sci 2012, 3, 1829–1834. [PubMed: 25431649]
34. Angelovski G; Toth E Strategies for Sensing Neurotransmitters with Responsive MRI Contrast Agents. Chem. Soc. Rev 2017, 46, 324–336. [PubMed: 28059423]
35. (a)Nahrendorf M; Sosnovik D; Chen JW; Panizzi P; Figueiredo JL; Aikawa E; Libby P; Swirski FK; Weissleder R Activatable Magnetic Resonance Imaging Agent Reports Myeloperoxidase Activity in Healing Infarcts and Noninvasively Detects the Antiinflammatory Effects of Atorvastatin on Ischemia-Reperfusion Injury. Circulation 2008, 117, 1153–1160; [PubMed: 18268141] (b)Rodriguez E; Nilges M; Weissleder R; Chen JW Activatable Magnetic Resonance Imaging Agents for Myeloperoxidase Sensing: Mechanism of Activation, Stability, and Toxicity. J. Am. Chem. Soc 2010, 132, 168–177; [PubMed: 19968300] (c)Su HS; Nahrendorf M; Panizzi P; Breckwoldt MO; Rodriguez E; Iwamoto Y; Aikawa E; Weissleder R; Chen JW Vasculitis: Molecular Imaging by Targeting the Inflammatory Enzyme Myeloperoxidase. Radiology 2012, 262, 181–190. [PubMed: 22084204]
36. (a)Ye DJ; Shuhendler AJ; Pandit P; Brewer KD; Tee SS; Cui LN; Tikhomirov G; Rutt B; Rao JH Caspase-Responsive Smart Gadolinium-Based Contrast Agent for Magnetic Resonance Imaging of Drug-Induced Apoptosis. Chem. Sci 2014, 5, 3845–3852;(b)Nejadnik H; Ye DJ; Lenkov OD; Donig JS; Martin JE; Castillo R; Derugin N; Sennino B; Rao JH; Daldrup-Link H Magnetic Resonance Imaging of Stem Cell Apoptosis in Arthritic Joints with a Caspase Activatable Contrast Agent. Acs Nano 2015, 9, 1150–1160; [PubMed: 25597243] (c)Shuhendler AJ; Ye DJ; Brewer KD; Bazalova-Carter M; Lee KH; Kempen P; Wittrup KD; Graves EE; Rutt B; Rao JH Molecular Magnetic Resonance Imaging of Tumor Response to Therapy. Sci. Rep 2015, 5.
37. Hai Z; Ni Y; Saimi D; Yang H; Tong H; Zhong K; Liang G Gamma-Glutamyltranspeptidase-Triggered Intracellular Gadolinium Nanoparticle Formation Enhances the T2-Weighted MR Contrast of Tumor. Nano Lett. 2019, 19, 2428–2433. [PubMed: 30856326]
38. (a)Bhorade R; Weissleder R; Nakakoshi T; Moore A; Tung CH Macrocyclic Chelators with Paramagnetic Cations Are Internalized into Mammalian Cells Via a Hiv-Tat Derived Membrane Translocation Peptide. Bioconjugate Chem. 2000, 11, 301–305;(b)Allen MJ; Meade TJ Synthesis and Visualization of a Membrane-Permeable MRI Contrast Agent. J. Biol. Inorg. Chem 2003, 8, 746–750; [PubMed: 14505078] (c)Allen MJ; MacRenaris KW; Venkatasubramanian PN; Meade TJ Cellular Delivery of MRI Contrast Agents. Chem. Biol 2004, 11, 301–307; [PubMed:

15123259] (d)Mishra R; Su W; Pohmann R; Pfeuffer J; Sauer MG; Ugurbil K; Engelmann J Cell-Penetrating Peptides and Peptide Nucleic Acid-Coupled MRI Contrast Agents: Evaluation of Cellular Delivery and Target Binding. Bioconjugate Chem. 2009, 20, 1860–1868.

39. (a)Rotz MW; Culver KSB; Parigi G; MacRenaris KW; Luchinat C; Odom TW; Meade TJ High Relaxivity Gd(III) - DNA Gold Nanostars: Investigation of Shape Effects on Proton Relaxation. Acs Nano 2015, 9, 3385–3396; [PubMed: 25723190] (b)Holbrook RJ; Rammohan N; Rotz MW; MacRenaris KW; Preslar AT; Meade TJ Gd(III)-Dithiolane Gold Nanoparticles for T-1-Weighted Magnetic Resonance Imaging of the Pancreas. Nano Lett. 2016, 16, 3202–3209; [PubMed: 27050622] (c)Nicholls FJ; Rotz MW; Ghuman H; MacRenaris KW; Meade TJ; Modo M DNA-Gadolinium-Gold Nanoparticles for in Vivo T1 Mr Imaging of Transplanted Human Neural Stem Cells. Biomaterials 2016, 77, 291–306; [PubMed: 26615367] (d)Rammohan N; Holbrook RJ; Rotz MW; MacRenaris KW; Preslar AT; Carney CE; Reichova V; Meade TJ Gd(III)-Gold Nanoconjugates Provide Remarkable Cell Labeling for High Field Magnetic Resonance Imaging. Bioconjugate Chem. 2017, 28, 153–160.
40. (a)Ghaghada KB; Ravoori M; Sabapathy D; Bankson J; Kundra V; Annapragada A New Dual Mode Gadolinium Nanoparticle Contrast Agent for Magnetic Resonance Imaging. PLoS One 2009, 4;(b)Tseng CL; Shih IL; Stobinski L; Lin FH Gadolinium Hexanedione Nanoparticles for Stem Cell Labeling and Tracking Via Magnetic Resonance Imaging. Biomaterials 2010, 31, 5427–5435; [PubMed: 20400176] (c)Guenoun J; Koning GA; Doeswijk G; Bosman L; Wielopolski PA; Krestin GP; Bernsen MR Cationic Gd-Dtpa Liposomes for Highly Efficient Labeling of Mesenchymal Stem Cells and Cell Tracking with MRI. Cell Transplant. 2012, 21, 191–205; [PubMed: 21929868] (d)Hung AH; Holbrook RJ; Rotz MW; Glasscock CJ; Mansukhani ND; MacRenaris KW; Manus LM; Duch MC; Dam KT; Hersam MC; Meade TJ Graphene Oxide Enhances Cellular Delivery of Hydrophilic Small Molecules by Co-Incubation. Acs Nano 2014, 8, 10168–10177; [PubMed: 25226566] (e)Rammohan N; MacRenaris KW; Moore LK; Parigi G; Mastarone DJ; Manus LM; Lilley LM; Preslar AT; Waters EA; Filicko A; Luchinat C; Ho D; Meade TJ Nanodiamond-Gadolinium(III) Aggregates for Tracking Cancer Growth in Vivo at High Field. Nano Lett. 2016, 16, 7551–7564. [PubMed: 27960515]
41. Gianolio E; Arena F; Strijkers GJ; Nicolay K; Hogset A; Aime S Photochemical Activation of Endosomal Escape of MRI-Gd-Agents in Tumor Cells. Magn. Reson. Med 2011, 65, 212–219. [PubMed: 21053327]
42. (a)Pan DPJ; Caruthers SD; Senpan A; Schmieder AH; Wickline SA; Lanza GM Revisiting an Old Friend: Manganese-Based MRI Contrast Agents. Wires Nanomed Nanobi 2011, 3, 162–173; (b)Pan DPJ; Schmieder AH; Wickline SA; Lanza GM Manganese-Based MRI Contrast Agents: Past, Present, and Future. Tetrahedron 2011, 67, 8431–8444; [PubMed: 22043109] (c)Drahos B; Lukes I; Toth E Manganese(Ii) Complexes as Potential Contrast Agents for MRI. Eur. J. Inorg. Chem 2012, 1975–1986;(d)Gale EM; Wey HY; Ramsay I; Yen YF; Sosnovik DE; Caravan P A Manganese-Based Alternative to Gadolinium: Contrast-Enhanced MR Angiography, Excretion, Pharmacokinetics, and Metabolism. Radiology 2018, 286, 877–884.
43. Barandov A; Badelle BB; Williamson CG; Loucks ES; Lippard SJ; Jasanoff A Sensing Intracellular Calcium Ions Using a Manganese-Based MRI Contrast Agent. Nat Commun 2019, 10. [PubMed: 30602777]
44. Stucht D; Danishad KA; Schulze P; Godenschweger F; Zaitsev M; Speck O Highest Resolution in Vivo Human Brain MRI Using Prospective Motion Correction. PLoS One 2015, 10.
45. Shapiro EM; Sharer K; Skrtic S; Koretsky AP In Vivo Detection of Single Cells by MRI. Magn. Reson. Med 2006, 55, 242–249. [PubMed: 16416426]
46. Hall LT; Hill CD; Cole JH; Stadler B; Caruso F; Mulvaney P; Wrachtrup J; Hollenberg LCL Monitoring Ion-Channel Function in Real Time through Quantum Decoherence. Proc. Natl. Acad. Sci. U. S. A 2010, 107, 18777–18782. [PubMed: 20937908]
47. Lilley LM; Du K; Krzyaniak MD; Parigi G; Luchinat C; Harris TD; Meade TJ Effect of Magnetic Coupling on Water Proton Relaxivity in a Series of Transition Metal Gd-III Complexes. Inorg. Chem 2018, 57, 5810–5819. [PubMed: 29714477]
48. (a)Ekanger LA; Polin LA; Shen Y; Haacke EM; Martin PD; Allen MJ A Eu-Ii-Containing Cryptate as a Redox Sensor in Magnetic Resonance Imaging of Living Tissue. Angew Chem Int Edit 2015, 54, 14398–14401;(b)Ekanger LA; Mills DR; Ali MM; Polin LA; Shen YM; Haacke EM; Allen MJ Spectroscopic Characterization of the 3+and 2+Oxidation States of Europium in a Macrocyclic

Tetraglycinate Complex. Inorg. Chem 2016, 55, 9981–9988; [PubMed: 27244124] (c)Gale EM; Jones CM; Ramsay I; Farrar CT; Caravan P A Janus Chelator Enables Biochemically Responsive MRI Contrast with Exceptional Dynamic Range. J. Am. Chem. Soc 2016, 138, 15861–15864; [PubMed: 27960350] (d)Basal LA; Bailey MD; Romero J; Ali MM; Kurenbekova L; Yustein J; Pautler RG; Allen MJ Fluorinated Eu-Ii-Based Multimodal Contrast Agent for Temperature- and Redox-Responsive Magnetic Resonance Imaging. Chem. Sci 2017, 8, 8345–8350; [PubMed: 29780447] (e)Wang H; Jordan VC; Ramsay IA; Sojoodi M; Fuchs BC; Tanabe KK; Caravan P; Gale EM Molecular Magnetic Resonance Imaging Using a Redox-Active Iron Complex. J. Am. Chem. Soc 2019, 141, 5916–5925. [PubMed: 30874437]

49. Frullano L; Catana C; Benner T; Sherry AD; Caravan P Bimodal Mr-Pet Agent for Quantitative pH Imaging. Angew Chem Int Edit 2010, 49, 2382–2384.
50. Gianolio E; Maciocco L; Imperio D; Giovenzana GB; Simonelli F; Abbas K; Bisi G; Aime S Dual MRI-Spect Agent for pH-Mapping. Chem. Commun 2011, 47, 1539–1541.
51. (a)Zhang XA; Lovejoy KS; Jasanoff A; Lippard SJ Water-Soluble Porphyrins as a Dual-Function Molecular Imaging Platform for MRI and Fluorescence Zinc Sensing. Proc. Natl. Acad. Sci. U. S. A 2007, 104, 10780–5; [PubMed: 17578918] (b)Tu C; Nagao R; Louie AY Multimodal Magnetic-Resonance/Optical-Imaging Contrast Agent Sensitive to Nadh. Angew Chem Int Edit 2009, 48, 6547–6551;(c)You YM; Tomat E; Hwang K; Atanasijevic T; Nam W; Jasanoff AP; Lippard SJ Manganese Displacement from Zinpyr-1 Allows Zinc Detection by Fluorescence Microscopy and Magnetic Resonance Imaging. Chem. Commun 2010, 46, 4139–4141;(d)Luo J; Li WS; Xu P; Zhang LY; Chen ZN Zn2+ Responsive Bimodal Magnetic Resonance Imaging and Fluorescent Imaging Probe Based on a Gadolinium(III) Complex. Inorg. Chem 2012, 51, 9508–9516; [PubMed: 22880548] (e)Zheng MM; Wang YQ; Shi H; Hu YX; Feng LD; Luo ZL; Zhou M; He J; Zhou ZY; Zhang Y; Ye DJ Redox-Mediated Disassembly to Build Activatable Trimodal Probe for Molecular Imaging of Biothiols. Acs Nano 2016, 10, 10075–10085. [PubMed: 27934082]
52. Li H; Parigi G; Luchinat C; Meade TJ Bimodal Fluorescence-Magnetic Resonance Contrast Agent for Apoptosis Imaging. J. Am. Chem. Soc 2019, 141, 6224–6233. [PubMed: 30919628]
53. Hung AH; Lilley LM; Hu FQ; Harrison VSR; Meade TJ Magnetic Barcode Imaging for Contrast Agents. Magn. Reson. Med 2017, 77, 970–978. [PubMed: 27062518]
54. Ma D; Gulani V; Seiberlich N; Liu K; Sunshine JL; Duerk JL; Griswold MA Magnetic Resonance Fingerprinting. Nature 2013, 495, 187–92. [PubMed: 23486058]
55. Anderson CE; Donnola SB; Jiang Y; Batesole J; Darrah R; Drumm ML; Brady-Kalnay SM; Steinmetz NF; Yu X; Griswold MA; Flask CA Dual Contrast-Magnetic Resonance Fingerprinting (DCMRF): A Platform for Simultaneous Quantification of Multiple MRI Contrast Agents. Sci. Rep 2017, 7. [PubMed: 28127057]

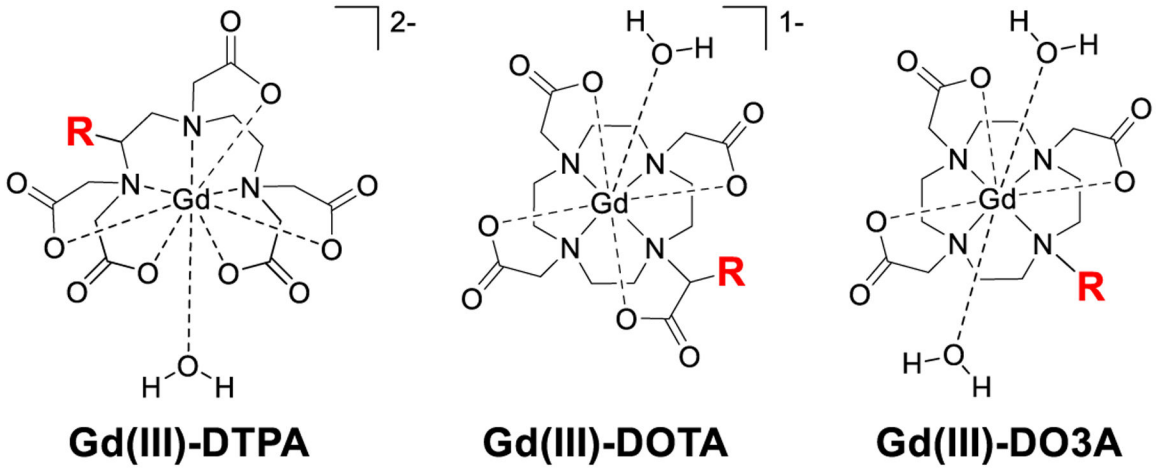

Figure 1.

Chemical structures of Gd(III)-DTPA, Gd(III)-DOTA and Gd(III)-DO3A. Different R groups (red) can be inserted to create bioresponsive GBCAs.

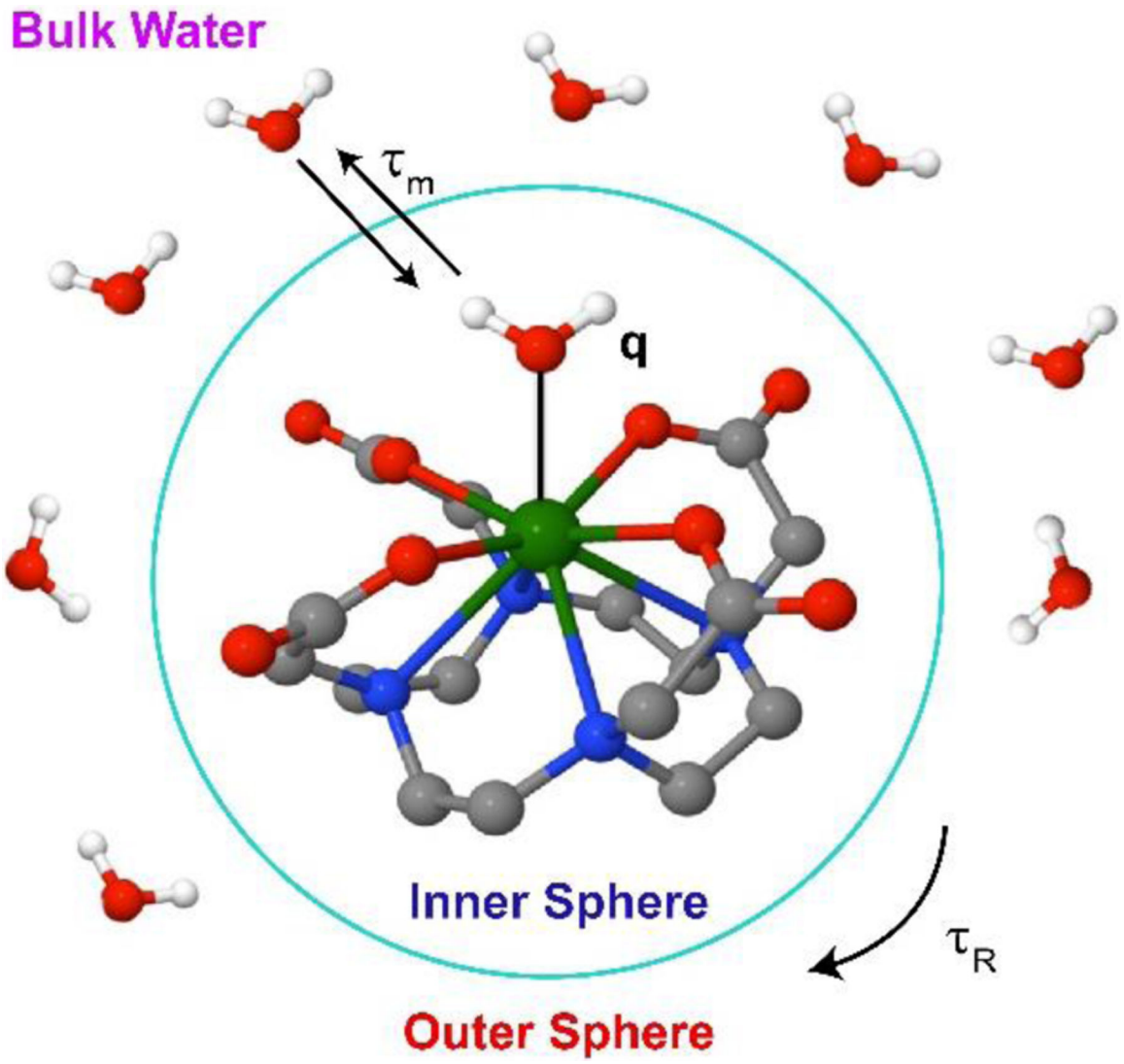

Figure 2.

Key parameters that affect inner-sphere relaxivity include hydration number (*q*), mean residence time of the bound water (τ_m), and rotational correlation time (τ_R).

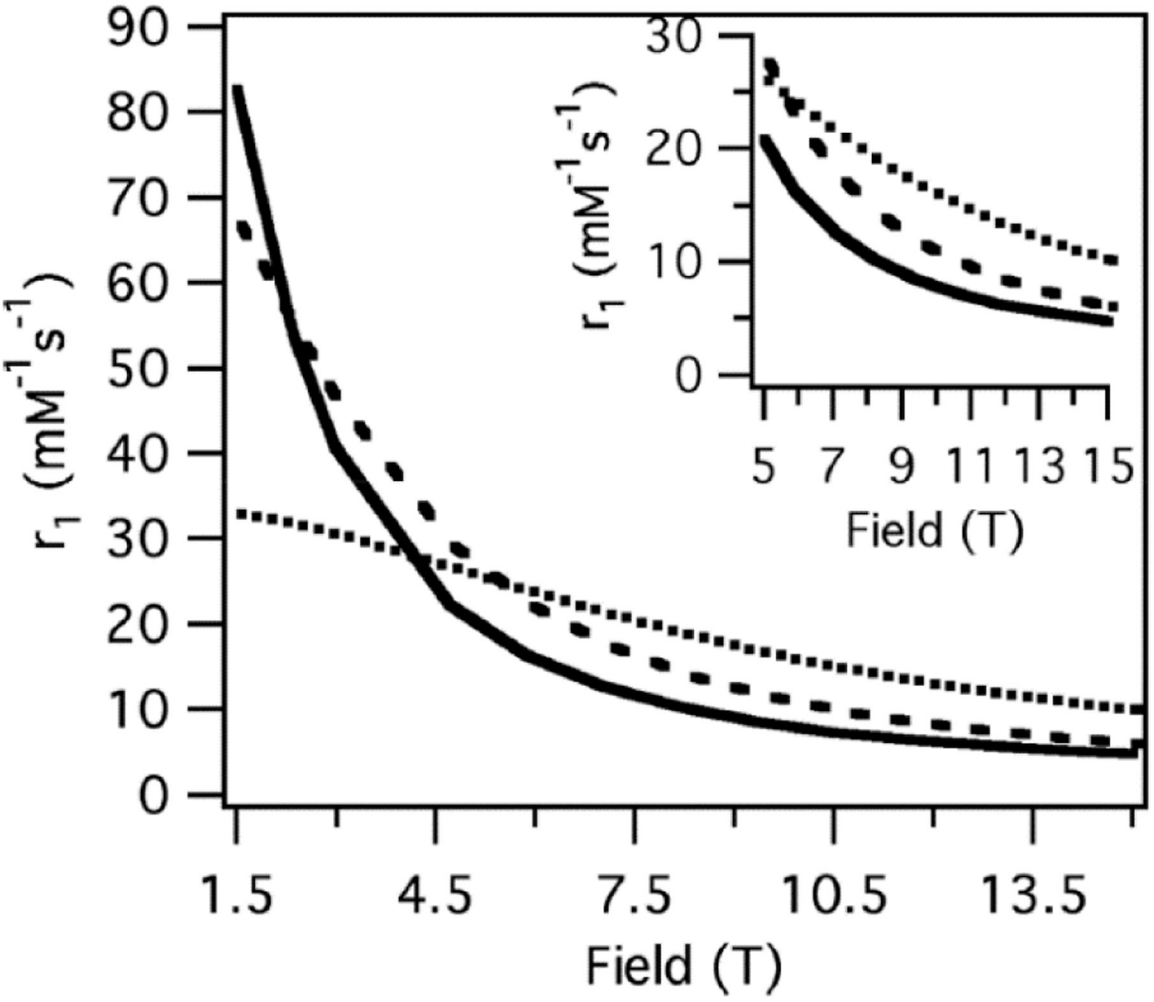

Figure 3.

Effect of rotational correlation time on r_1 as a function of field for a Gd(III) complex with a water residency time 100 ns. τ_R = 0.1 ns (···), 1.0 ns (---), 10 ns (—). At low field (1.5 T), long τ_R (10 ns) gives the highest r_1. However, at high field, the intermediate τ_R (1 ns) gives the highest r_1. Reproduced with permission from ref 13. Copyright 2009 John Wiley and Sons.

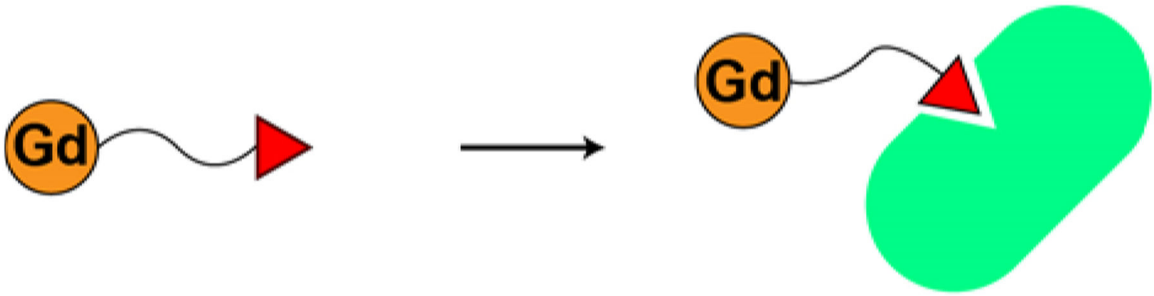

Figure 4.

Depiction for targeted GBCAs. Upon binding the target biomarker, the GBCAs exhibit enhanced retention *in vivo* as well as increased r_1 due to RIME effect.

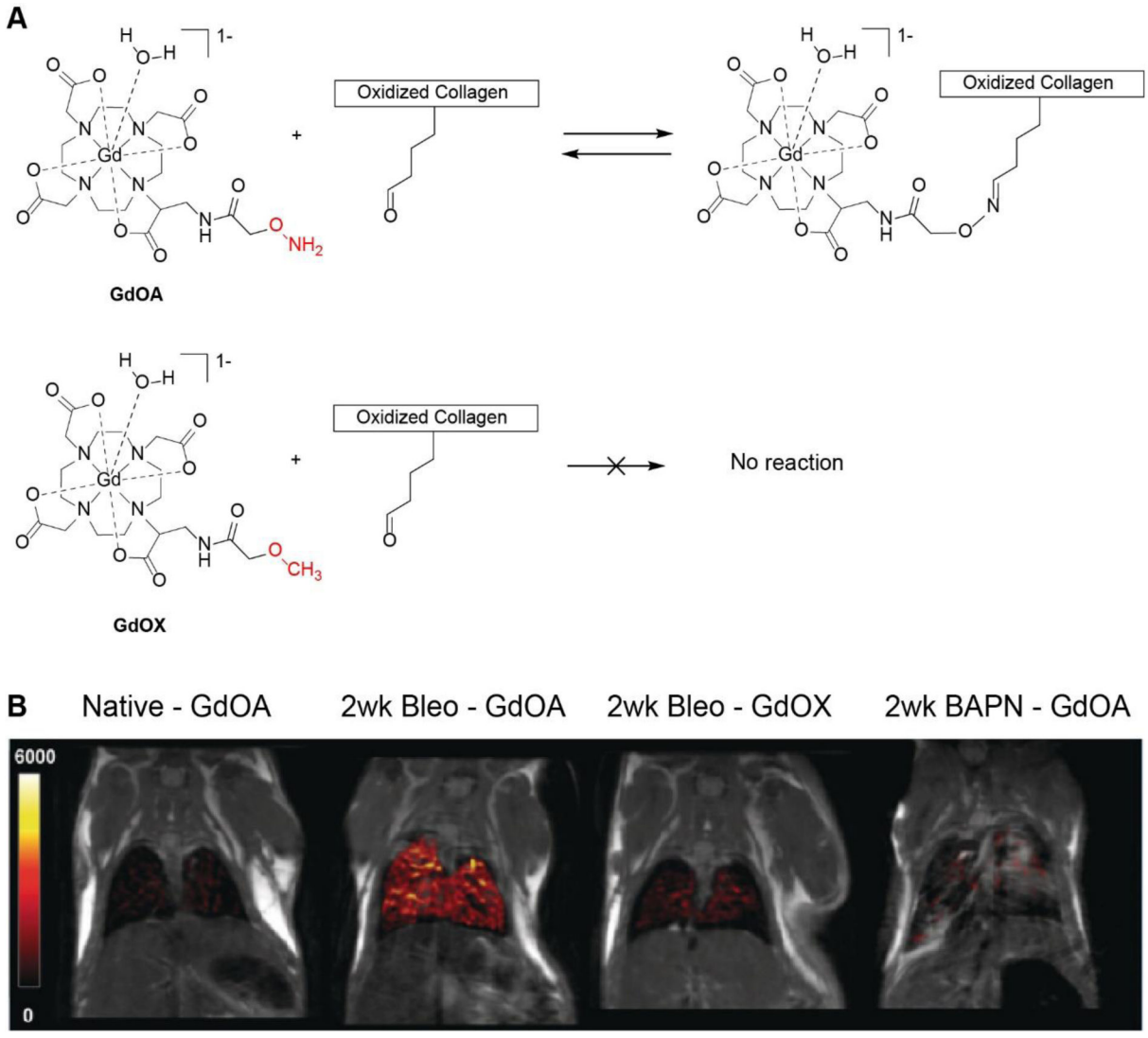

Figure 5.

(A) Chemical structure and targeting mechanism of GdOA. GdOA has an oxyamine group that can reversibly bind to allysine present in oxidized collagen. GdOX is a control probe that does not interact with allysine. (B) Coronal MR images (9.4 T) of normal and bleomycin injured mice injected with GdOA or GdOX. Bleomycin injured mice injected with GdOA (2nd) clearly showed an enhanced MR signal in the lung compared to normal mice injected with GdOA (1st) or injured mice injected with the control probe GdOX (3rd). In the last image, β-aminopropionitrile (BAPN) which inhibits allysine production was used in bleoinjured mice, and little MR signal enhancement was seen when mice were injected with GdOA. Reproduced with permission from ref 19. Copyright 2017 John Wiley and Sons.

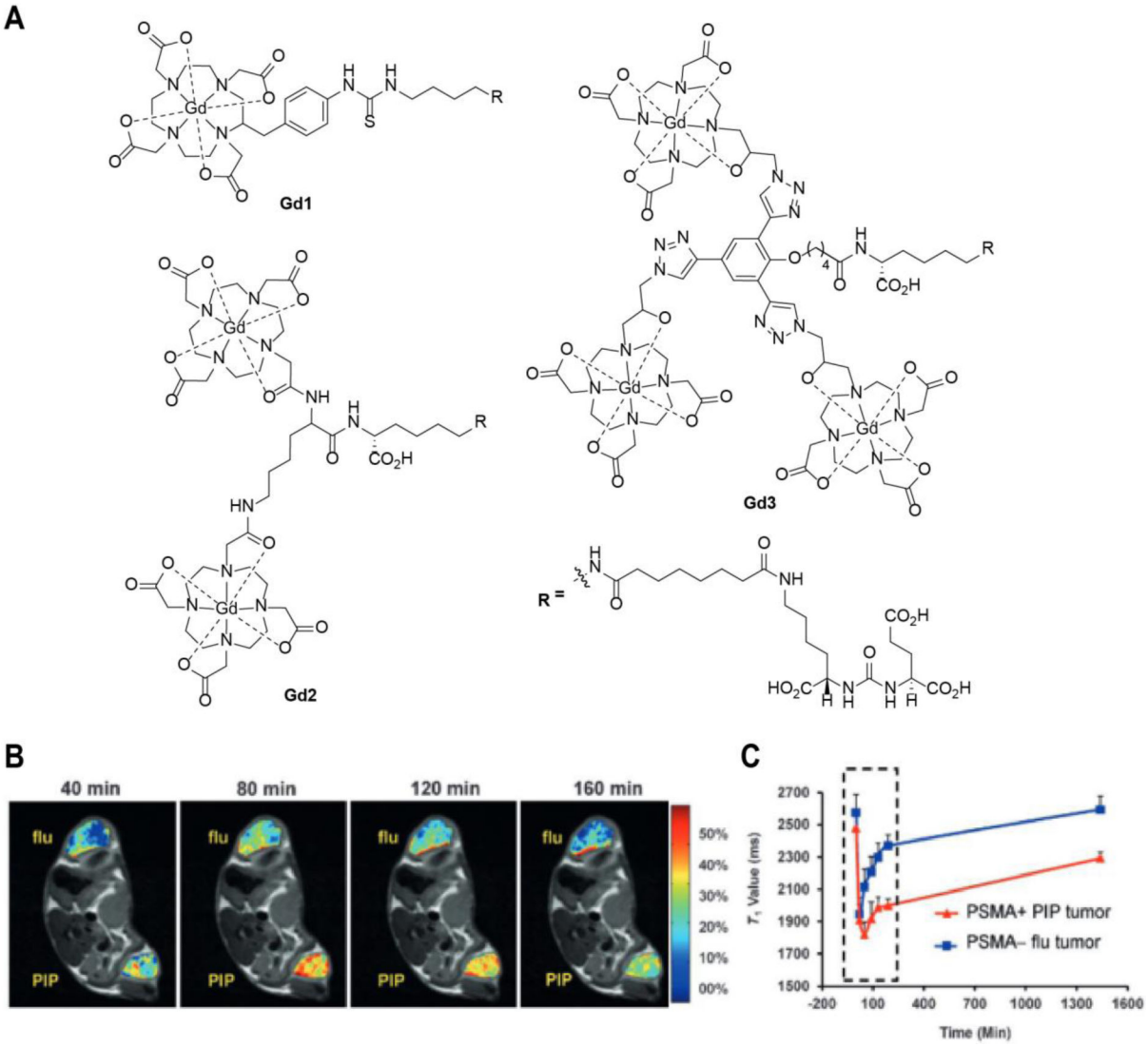

Figure 6.

(A) Chemical structures of PSMA targeting GBCAs, Gd1, Gd2, Gd3. The R group is the targeting ligand for PSMA. (B) T_1-weighted MR signal enhancement map (9.4 T) in PC3 PIP (PSMA+) and PC3 flu (PSMA-) tumors superimposed upon T_2-weighted images after the mice were injected with Gd3. (C) T_1 time courses calculated for the entire volume of each tumor during 1–1600 min post injection. Gd3 was retained in the PSMA+ PIP tumor in the first 3hrs but was quickly washed out from PSMA-flu tumor. Reproduced with permission from ref 20. Copyright 2017 John Wiley and Sons.

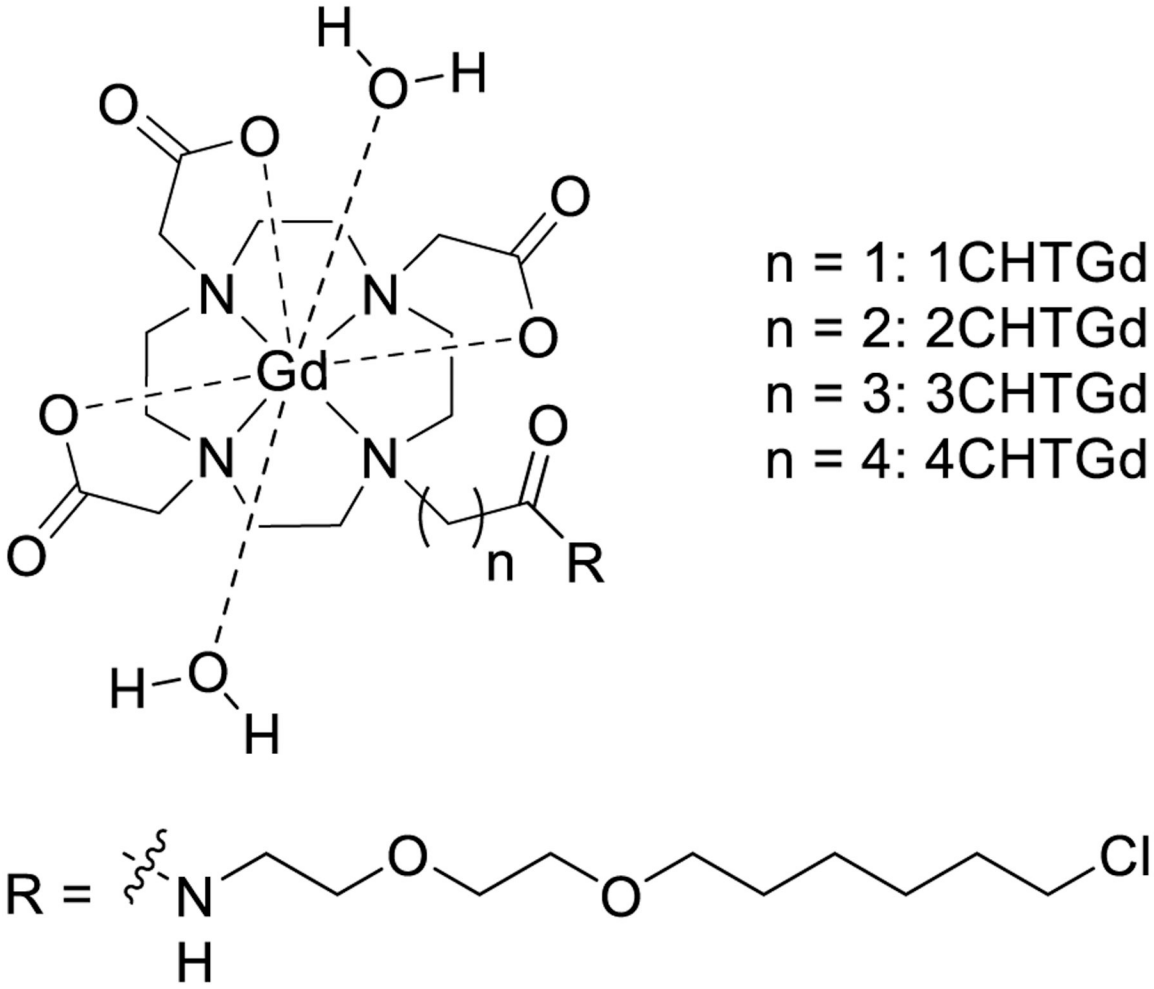

Figure 7.

Chemical structures of HaloTag targeting GBCAs of different linker length. 2CHTGd has both optimal binding and maximal relaxivity increase upon binding.

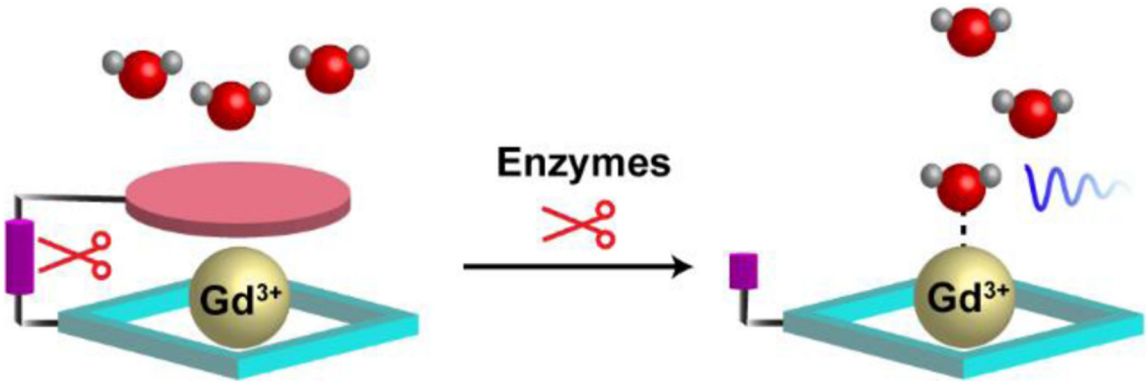

Figure 8.

Pictorial depiction for activatable GBCAs that can be used to image enzyme activities. Upon cleavage of the capping ligand, the inner-sphere relaxivity is increased as water access to the metal center is resumed.

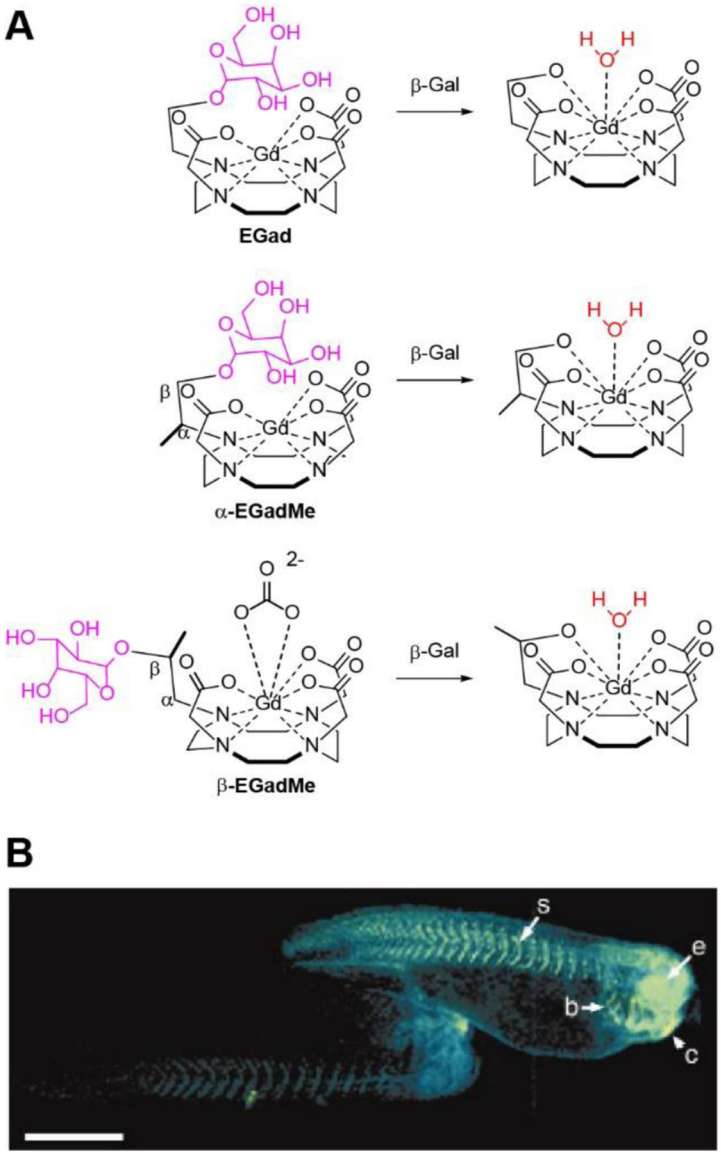

Figure 9.

(A) Chemical structures of β-galactosidase-responsive GBCAs: Egad, α-EGadMe and β-EGadMe. (B) MRI (11.7 T) detection of β-galactosidase mRNA expression in living X. laevis embryos injected with EgadMe at the two-cell stage. The embryo on the right was also injected with β-gal mRNA, resulting in higher MR signal in certain regions. s, somite; b, brachial arches; e, eye; c, cement gland. Scale bar = 1 mm. Reproduced with permission from ref 27a. Copyright 2000 Springer Nature.

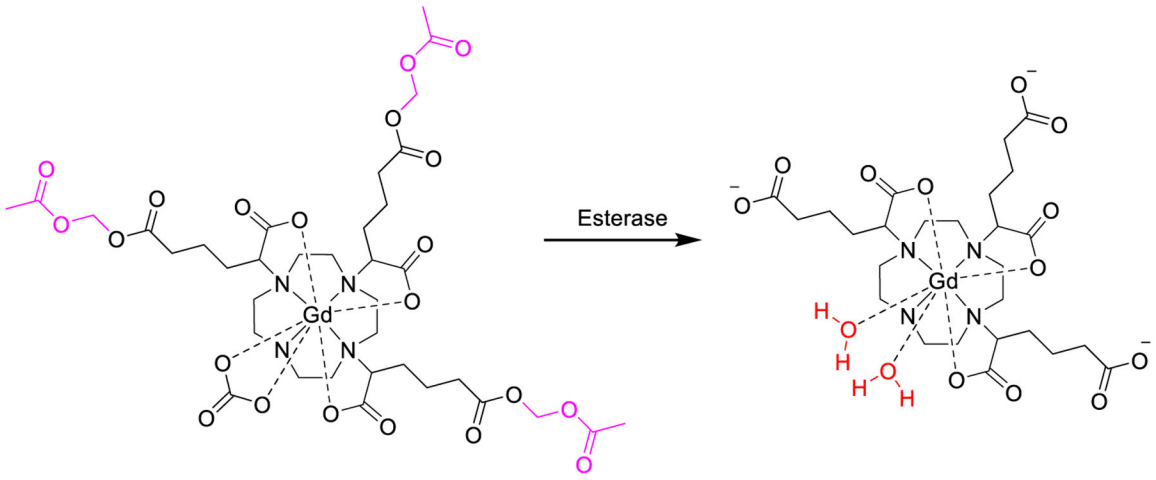

Figure 10.

Activatable GBCA for detecting esterase activities. Esterase unmasks the carboxylate groups which repels the carbonate binding to the Gd(III) metal center.

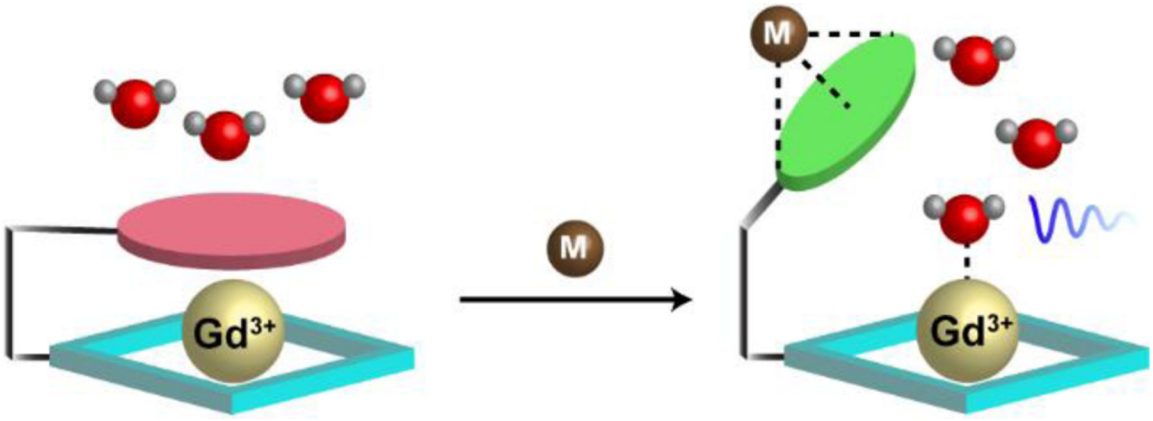

Figure 11.

Pictorial depiction for activatable GBCAs for sensing metal ions. Upon binding of the target metal ion, the capping ligand is lifted leading to increased *q* and hence higher inner-sphere relaxivity.

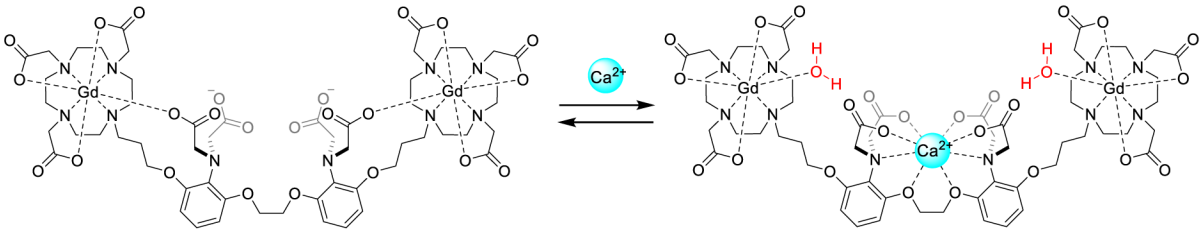

Figure 12.

Chemical structure of the Ca(II)-sensitive GBCA, DOPTA–Gd. The BAPTA core is responsible for binding with Ca(II) of physiologically relevant concentration, leading to increased q and hence higher r_1.

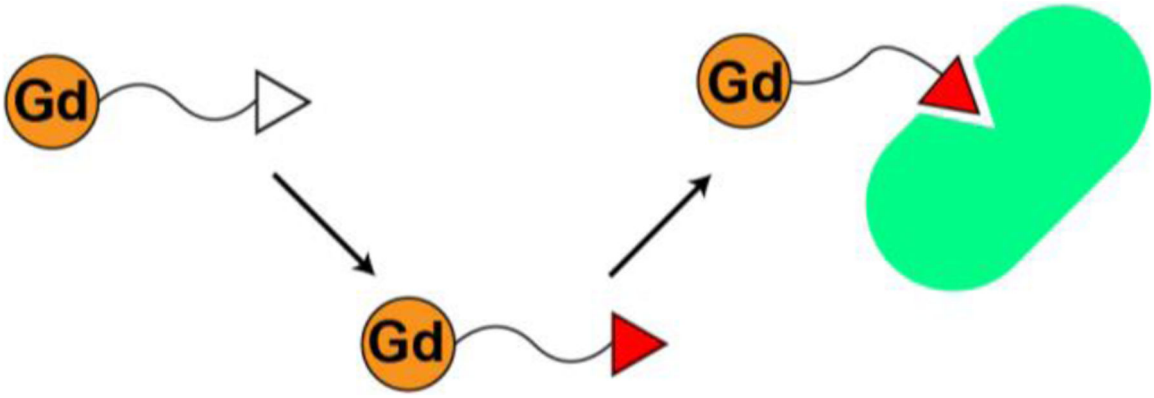

Figure 13.

Pictorial depiction for activation-binding mechanism. These GBCAs are first conditionally activated which then acquired the ability to bind to proteins such as serum albumin, leading to increased r_1 and retention.

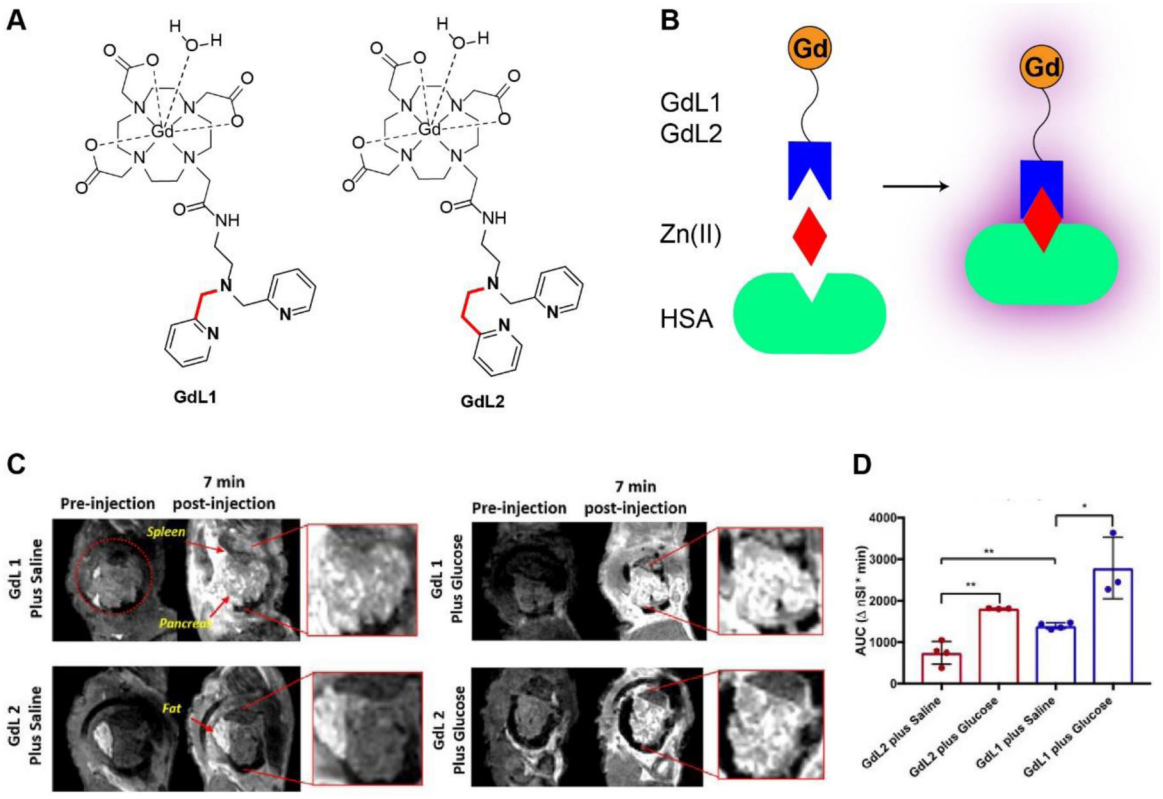

Figure 14.

(A) Chemical structures of Zn(II)-sensitive GBCAs that upon binding with Zn(II) acquire the ability to interact with HSA. GdL2 has lower affinity towards Zn(II) than GdL1. (B) Pictorial depiction of the activation-binding mechanism of GdL1 and GdL2. (C) 3D T_1-weighted MRI (9.4 T) of mouse pancreas pre- and postdelivery of GdL1 or GdL2 plus saline or glucose. Glucose stimulates the release of Zn(II) from β-cells in the pancreas, whereas saline serves as a vehicle control. (D) average MR from 0 to 28 min for saline-treated mice (n = 4) and for glucose-treated animals. Although GdL1 gave higher signal under glucose stimulation, GdL2 had lower signal background when only saline was injected. This was attributed to the lower affinity of GdL2 towards background Zn(II) in the tissue. Bars represent the standard error of the mean; *p-value < 0.05, **p-value < 0.01 Reproduced with permission from ref 18f. Copyright 2018 American Chemical Society.

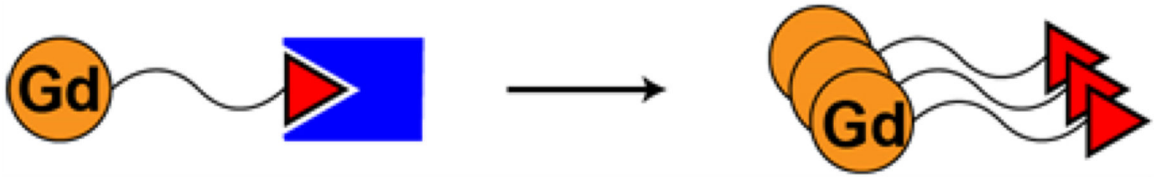

Figure 15.

Pictorial depiction for activatable GBCAs that based on responsive self-assemble or aggregation. Note that these agents usually are better retained post-activation, as larger particles tend to have a slower clearance rate.

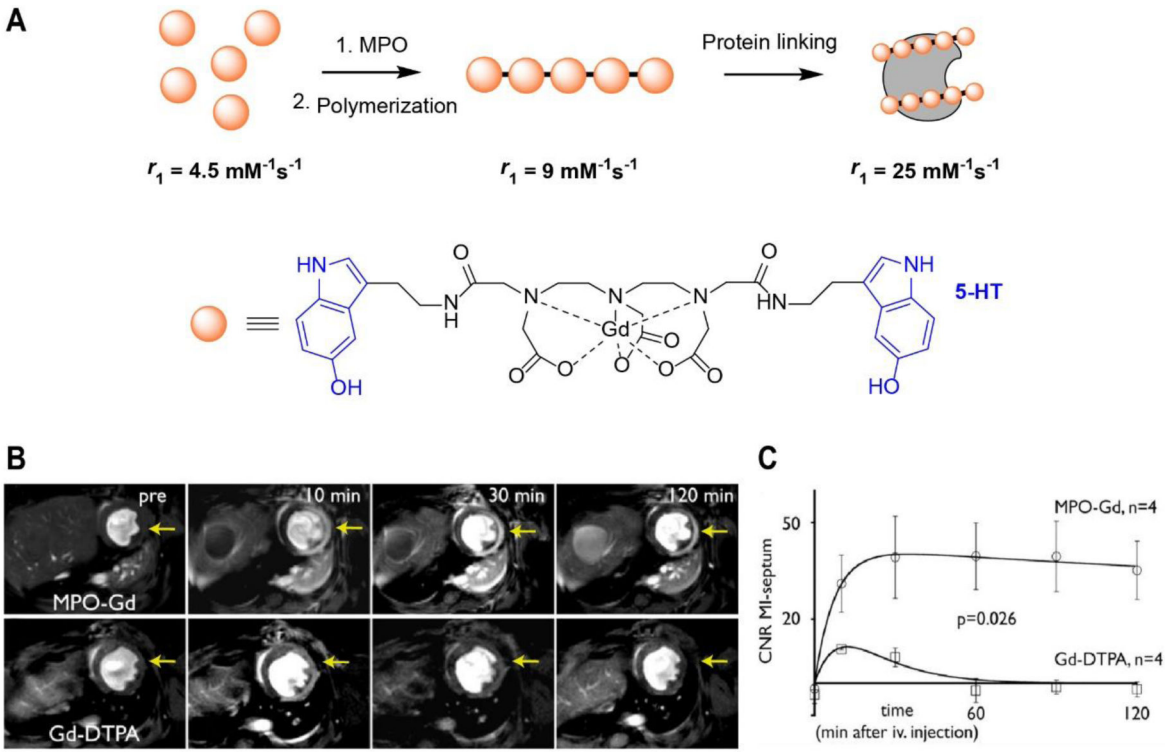

Figure 16.

(A) Chemical structures of MPO-sensitive GBCAs, MPO-Gd. In the presence of MPO, the 5-HT moiety is oxidized to form radicals, leading to oligomerization of the MPO-Gd as well as linking to surrounding proteins. (B) *In vivo* MRI (7 T) of MPO activity 2 days after myocardial infarction was induced. Strong and persistent MR signal enhancement was seen in the infarct zone (denoted by the yellow arrow) in mice injected with MPO-Gd, but not with Gd(III)-DTPA (C) The signal-to-noise ratio (SNR) showed higher values and stronger retention after injection of MPO-Gd compared to Gd(III)-DTPA. Reproduced with permission from ref 35a. Copyright 2008 Wolters Kluwer Health, Inc.

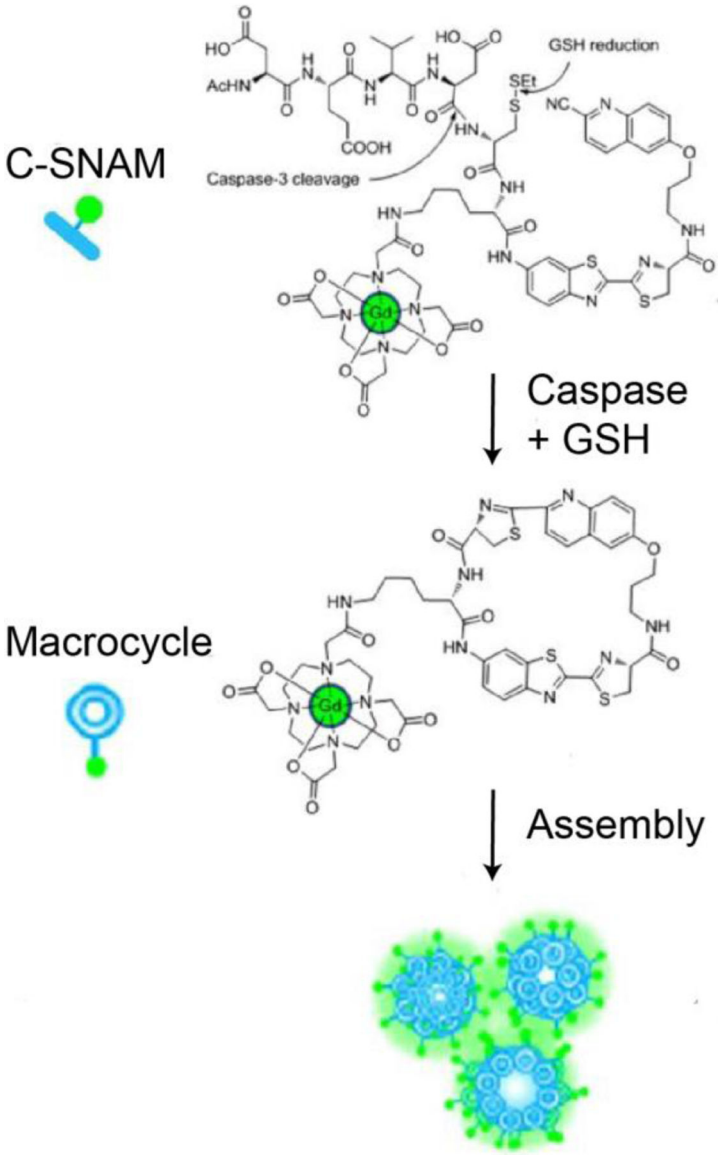

Figure 17.

Caspase-3/7 responsive GBCA, C-SNAM, is activated by cleavage of the DEVD peptide by caspase-3/7 and disulfide exchange with intracellular GSH. It then undergoes a biocompatible intramolecular cyclization to form a rigid and hydrophobic macrocycle. Reproduced with permission from ref 36b. Copyright 2015 American Chemical Society.

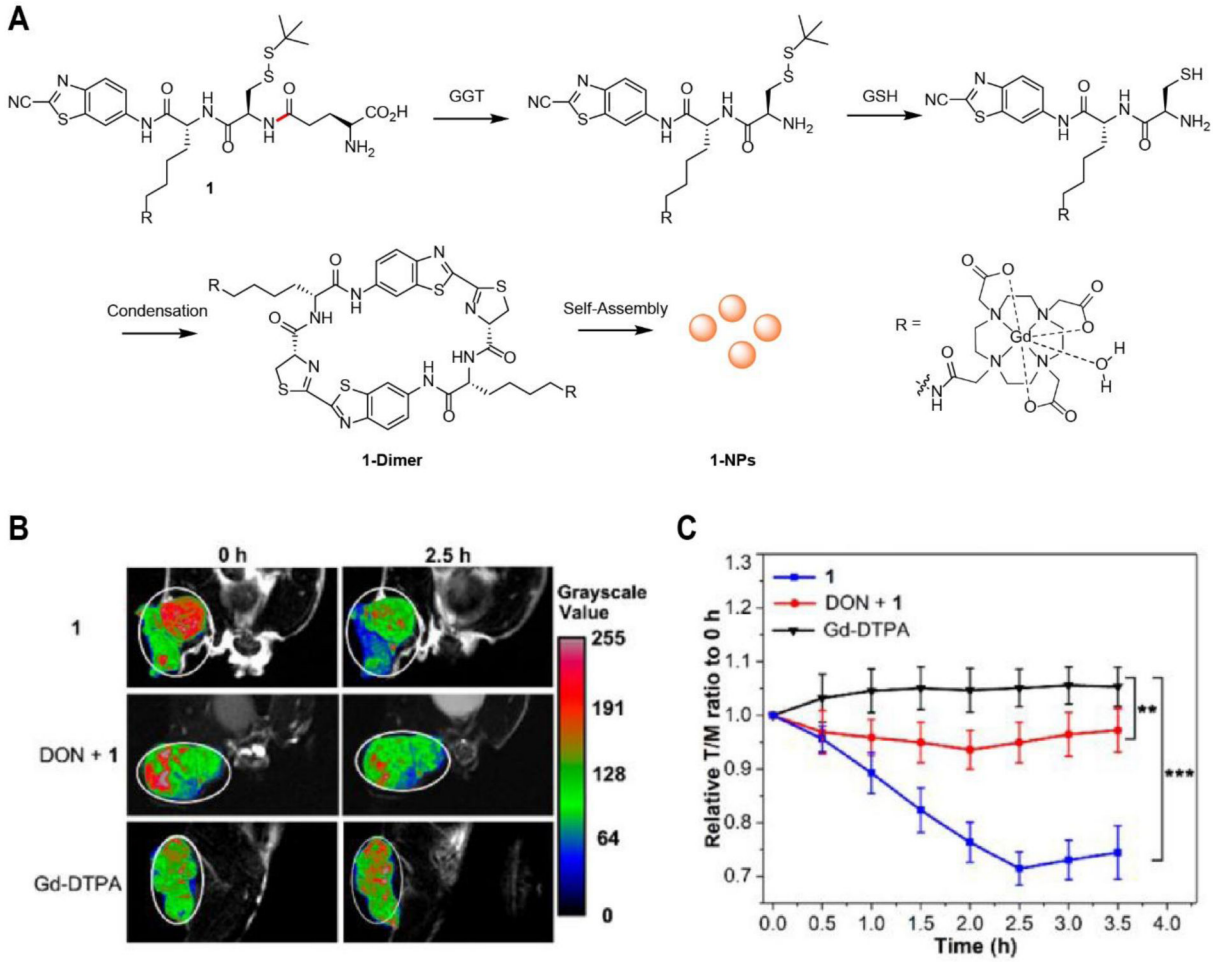

Figure 18.

(A) GGT-responsive GBCA, 1, is activated by cleavage of the glutamate by GGT and disulfide exchange with intracellular GSH. It then dimerizes to form a rigid and hydrophobic macrocycle, whichself-assembles into nanoparticles (B) T_2-weighted coronal MRI (9.4 T) of HeLa tumor bearing mice intravenously injected with 1 (top row), DON for 0.5 h and then 0.08 mmol/kg (middle row), and 0.08 mmol/kg Gd(III)-DTPA (bottom row) at 0 h and 2.5 hrs. (C) Normalized time course tumor-to-muscle (T/M) contrast ratios of T_2 values in panel B. Significant T_2 reduction was observed with Hela-bearing mice 2.5 hrs post injection with 1. Each error bar represents the standard deviation of three independent experiments. *p < 0.05, **p < 0.01, ***p < 0.001; analyzed by Student's t-test. Reproduced with permission from ref 37. Copyright 2019 American Chemical Society.

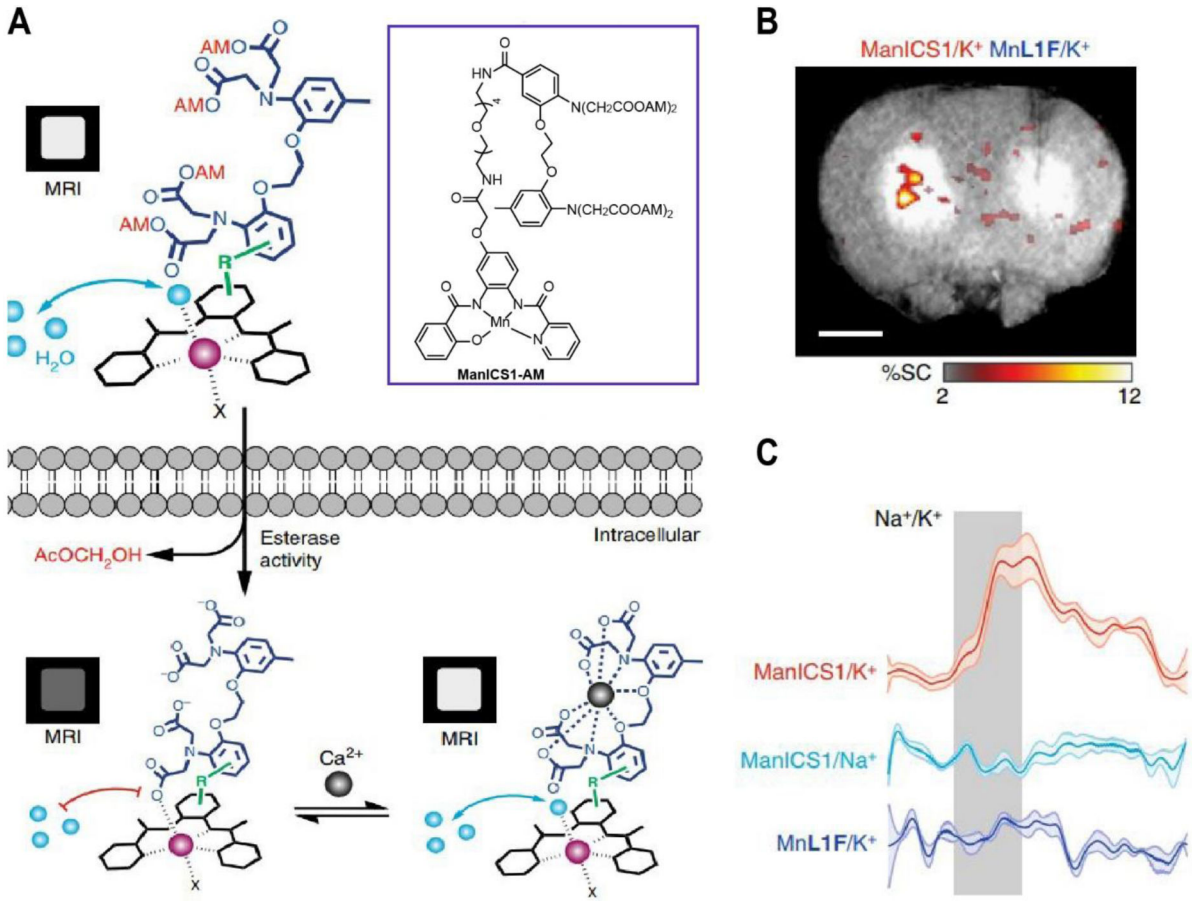

Figure 19.

(A) Manganese-based intracellular calcium sensor (ManICS1-AM) is cell permeable. When the agent enters cells, the AM esters are cleaved by intracellular esterases. This liberates the "off-state", which can interact with intracellular Ca^{2+} and turns on the MR signal. (B) 1 μL K^+ infusion causes T_1-weighted MR signal (9.4 T) to increase in the presence of pre-delivered ManICS1-AM (left) but not MnL1F (right), a calcium-insensitive control. Average peak signal change across multiple animals (n = 5) is indicated by the color scale superimposed on a high resolution T_1-weighted image of a representative rat. Scale bar = 3 mm. (C) Region of interest analysis shows the time course of signal changes observed during K^+ or Na^+ in the presence of ManICS1 (red and cyan, respectively), and during K^+ stimulation (vertical gray bar) in the presence of calcium-insensitive MnL1F (blue). Reproduced from ref 42. Distributed under the terms of the Creative Commons CC BY license.

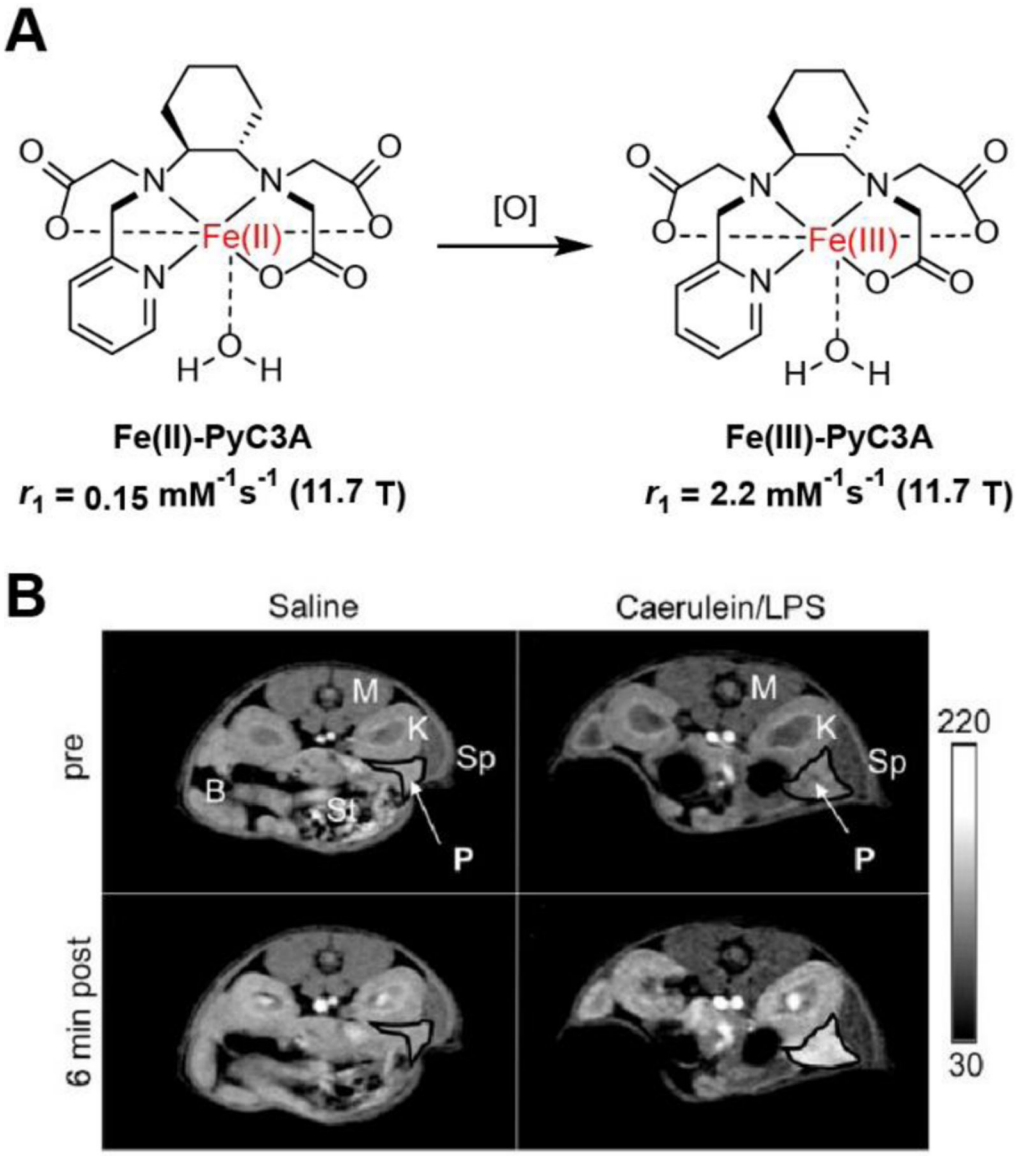

Figure 20.

(A) Fe-based redox-sensitive MRCA Fe(II)-Pyc3A has low r_1 due to diamagnetic Fe(II). In oxidative environment the Fe(II) is oxidized to Fe(III) that is paramagnetic. As a result, a large $r_1$increase was achieved. (B) T_1-weighted 2D axial images (4.7 T) of saline and caerulein/LPS treated mice recorded prior to and 6 min after injection of 0.2 mmol/kg Fe(II)-PyC3A. Organs are labeled as follows: P = pancreas, Sp = spleen, K = kidney, M = muscle, St = stomach, B = bowel. Note that the pancreas and neighboring kidney are virtually isointense prior to probe injection (top two images). After injection of Fe(II)-PyC3A to saline treated mice the pancreas and kidney remain isointense (bottom left), but that the pancreas is strongly and selectively enhanced after injection of Fe(II)-PyC3A to caerulein/LPS treated mice (bottom right). Reproduced with permission from ref 48e. Copyright 2019 American Chemical Society.